



---

MSU Graduate Theses

---

Spring 2020

## Determining Particle Size of Polymeric Micelles in Thermothickening Aqueous Solutions


Jessica Diane Bruer

Missouri State University, [Jessica1897@live.missouristate.edu](mailto:Jessica1897@live.missouristate.edu)

As with any intellectual project, the content and views expressed in this thesis may be considered objectionable by some readers. However, this student-scholar's work has been judged to have academic value by the student's thesis committee members trained in the discipline. The content and views expressed in this thesis are those of the student-scholar and are not endorsed by Missouri State University, its Graduate College, or its employees.

---

Follow this and additional works at: <https://bearworks.missouristate.edu/theses>

 Part of the [Physical Chemistry Commons](#), and the [Polymer Chemistry Commons](#)

### Recommended Citation

Bruer, Jessica Diane, "Determining Particle Size of Polymeric Micelles in Thermothickening Aqueous Solutions" (2020). *MSU Graduate Theses*. 3472.

<https://bearworks.missouristate.edu/theses/3472>

This article or document was made available through BearWorks, the institutional repository of Missouri State University. The work contained in it may be protected by copyright and require permission of the copyright holder for reuse or redistribution.

For more information, please contact [BearWorks@library.missouristate.edu](mailto: BearWorks@library.missouristate.edu).

**DETERMINING PARTICLE SIZE OF POLYMERIC MICELLES IN  
THERMOTHICKENING AQUEOUS SOLUTIONS**

A Master's Thesis

Presented to

The Graduate College of

Missouri State University

In Partial Fulfillment

Of the Requirements for the Degree

Master of Science, Chemistry

By

Jessica Diane Bruer

May 2020

Copyright 2020 by Jessica Diane Bruer

# DETERMINING PARTICLE SIZE OF POLYMERIC MICELLES IN THERMOTHICKENING AQUEOUS SOLUTIONS

Chemistry

Missouri State University, May 2020

Master of Science

Jessica Bruer

## ABSTRACT

Many active pharmaceutical ingredients (APIs) are poorly soluble and cause inadequate drug absorption. Soluplus<sup>®</sup>, a polyvinyl caprolactam-polyvinyl acetate-polyethylene glycol graft copolymer, is a commercial excipient (BASF Corp) that enhances the solubility and bioavailability of many APIs. The mechanism of enhancement is related to the ability to form polymeric micelles in solution. These micelles store insoluble APIs in their hydrophobic interior and transport them to targeted sites in the body. An important characteristic of solubility enhancers is the particle size exhibited in solution before and after loading with APIs. This is most commonly determined by dynamic light scattering (DLS) methods. However, DLS measurements involving thermothickening polymer solutions can be complicated by the temperature dependence of viscosity and refractive index, solution properties that directly impact the size analysis algorithms in DLS. In this project, the temperature dependence of viscosity for Soluplus<sup>®</sup> solutions were evaluated and used as a correction to particle size measurements by DLS. Solution concentrations ranging 1.0% to 30.0% (w/w) of Soluplus<sup>®</sup> were studied from 5.0 °C to 40.0 °C using a cone-and-plate rheometer. Refractive index of Soluplus<sup>®</sup> solutions were also studied and used in the correction of particle size. It was found that correcting viscosity and refractive index data drastically affected hydrodynamic effective diameter, where viscosity was more highly weighted. The corrected particle size of Soluplus<sup>®</sup> solutions was inversely proportional to concentration with the 0.1% and 10.0% solutions showing effective diameters of  $63.13 \pm 0.76$  nm and  $24.98 \pm 0.30$  nm at 25.0 °C, respectively. By properly accounting for these variables in DLS algorithms, particle size of thermoresponsive polymer solutions can be more accurately characterized.

**KEYWORDS:** rheology, dynamic light scattering, Soluplus<sup>®</sup>, thermoresponsive, block copolymer, active pharmaceutical ingredient, viscosity, refractive index, thermothickening, polymeric micelles

**DETERMINING PARTICLE SIZE OF POLYMERIC MICELLES IN  
THERMOTHICKENIG AQUEOUS SOLUTIONS**

By

Jessica Bruer

A Master's Thesis  
Submitted to the Graduate College  
Of Missouri State University  
In Partial Fulfillment of the Requirements  
For the Degree of Master of Science, Chemistry

May 2020

Approved:

G. Alan Schick, Ph.D., Thesis Committee Chair

Gary Meints, Ph.D., Committee Member

Ridwan Sakidja, Ph.D., Committee Member

Adam Wanekaya, Ph.D., Committee Member

Julie Masterson, Ph.D., Dean of the Graduate College

In the interest of academic freedom and the principle of free speech, approval of this thesis indicates the format is acceptable and meets the academic criteria for the discipline as determined by the faculty that constitute the thesis committee. The content and views expressed in this thesis are those of the student-scholar and are not endorsed by Missouri State University, its Graduate College, or its employees.

## ACKNOWLEDGEMENTS

I would like to thank those who showed their support during the course of my graduate studies. Specially my family, who endlessly support my decisions. Without their encouragement I would not be where I am today. A special thank you to my siblings, Kyle Bruer and Alyssa Mansfield, for pushing me to be my best in hopes I'd be as successful as they are. To my future sister-in-law, Jill Davis, I greatly appreciated the help and patience with data manipulation. I am upmost grateful for the support of my parents, Richard and Theresa Bruer, who have taught me that no ambition is too grand. Thank you for always being my cheerleaders and helping me at any cost.

I would also like to thank my research advisor, Dr. G. Alan Schick, who has guided me since my undergraduate years. I appreciate his commitment to furthering my education and introducing me to physical chemistry. Additionally, I thank my thesis committee for their time and support: Dr. Gary Meints, Dr. Ridwan Sakidja, and Dr. Adam Wanekaya. I am tremendously grateful for the friends I have made throughout this journey: fellow graduate students, research members, and faculty, who made coming to campus enjoyable and entertaining. Specifically, Cody Turner who has been my rock through our entire accelerated master's journey together.

I dedicate this thesis to my mother, Theresa Bruer, for sparking my interest in science with participation in the elementary school science fairs.

## TABLE OF CONTENTS

Chapter 1. Introduction	Page 1
1.1 Poor Solubility in the Pharmaceutical Field	Page 1
1.2 Polymers	Page 1
1.2.1 Polymer Behavior	Page 2
1.2.2 Function with Active Pharmaceutical Ingredients	Page 3
1.3 Thermoresponsivity	Page 4
1.4 Soluplus <sup>®</sup>	Page 7
1.5 Dynamic Light Scattering Spectroscopy	Page 14
1.5.1 Effect of Viscosity	Page 14
1.5.2 Effect of Refractive Index	Page 20
1.6 Objectives	Page 21
 Chapter 2. Experimental	 Page 22
2.1 Overview	Page 22
2.2 Materials	Page 22
2.3 Temperature Dependence of Viscosity	Page 23
2.3.1 Instrumentation	Page 23
2.3.2 Methods	Page 27
2.4 Refractive Index Analysis	Page 28
2.4.1 Instrumentation	Page 28
2.4.2 Methods	Page 29
2.5 Particle Size Determination by Dynamic Light Scattering	Page 30
2.5.1 Instrumentation	Page 30
2.5.2 Methods	Page 33
 Chapter 3. Results and Discussion	 Page 35
3.1 Temperature Dependent Viscoelastic Behavior of Soluplus <sup>®</sup> Solutions	Page 35
3.2 Temperature Dependent Refractive Index of Soluplus <sup>®</sup> Solutions	Page 47
3.3 Particle Size Analysis of Soluplus <sup>®</sup> Solutions	Page 48
 Chapter 4. Conclusions and Future Directions	 Page 55
 References	 Page 58

## LIST OF TABLES

Table 1. Types and examples of copolymers	Page 2
Table 2. Approximate viscosity values of commonly known materials at 20.0 °C	Page 18
Table 3. Cone spindle dimensions and shear rates	Page 26
Table 4. Experimental conditions for each sample/standard run on the rheometer	Page 28
Table 5. Temperatures used in the evaluation of refractive index for various standards and samples	Page 30
Table 6. Standard operating procedures for temperature dependent particle size analysis	Page 34
Table 7. Total allowed error for each viscosity standard fluid at 25.0 °C	Page 35
Table 8. Extrema temperatures observed in $\eta$ - $T$ plots of Soluplus <sup>®</sup> solutions	Page 39
Table 9. Experimental and literature refractive index values for water and ethanol at 20.0 °C	Page 47
Table 10. Effective diameters of NIST latex calibration standards at 25.0 °C	Page 49
Table 11. Uncorrected vs. corrected effective diameters at 25.0 °C for Soluplus <sup>®</sup> in aqueous solution	Page 52
Table 12. Difference in effective diameter when using uncorrected and corrected viscosity and refractive index data for a 10.0% Soluplus <sup>®</sup> solution at 20.0 °C	Page 53
Table 13. Effective diameter dependence on refractive index for a 10.0% Soluplus <sup>®</sup> solution at 20.0 °C and 5.842 cP	Page 54



## LIST OF FIGURES

Figure 1. Structure of a polymeric micelle with APIs stored in its core	Page 4
Figure 2. Temperature vs. polymer volume fraction ( $\phi$ ) plots	Page 6
Figure 3. Schematic representation of block copolymer phase transitions	Page 7
Figure 4. Physical appearance of Soluplus <sup>®</sup>	Page 8
Figure 5. Structure of Soluplus <sup>®</sup>	Page 9
Figure 6. Solubilization capacities of various active pharmaceutical ingredients	Page 10
Figure 7. Dissolution test for the release of itraconazole with polymeric matrices	Page 10
Figure 8. Blood concentration of itraconazole with and without Soluplus <sup>®</sup> solution	Page 10
Figure 9. Phase diagram for a LCST < UCST behaving polymer	Page 12
Figure 10. Micellization mechanism for solutions of Soluplus <sup>®</sup>	Page 13
Figure 11. Soluplus <sup>®</sup> solution at room temperature, cloud point, and gel point	Page 13
Figure 12. Particle size data for a pigment dispersed in water at two different viscosities	Page 15
Figure 13. Two plates model used to describe the physics of viscosity	Page 17
Figure 14. Graphical relationship between complex shear modulus $G^*$ , storage moduli $G'$ , loss moduli $G''$ , and the phase-shift angle $\delta$	Page 20
Figure 15. Schematics of a cone-and-plate rheometer	Page 25
Figure 16. Diagram of the inner workings of the cone and plate	Page 25
Figure 17. Top view of spindles CP40 and CP52	Page 26
Figure 18. Set-up used for viscosity data collection on a Brookfield rheometer	Page 28
Figure 19. Set-up used for refractive index data collection on an Abbe refractometer	Page 29
Figure 20. Shadow and scale within an Abbe-type refractometer	Page 30
Figure 21. Schematic representation of the Zetasizer Nano series DLS instrument	Page 31
Figure 22. Set-up used for particle size data collection on a NanoBrook Omni	Page 33
Figure 23. Brookfield viscosity standard fluids as a function of temperature	Page 35
Figure 24. Effect of temperature on viscosity for each aqueous Soluplus <sup>®</sup> sample	Page 37
Figure 25. Viscosity of Soluplus <sup>®</sup> samples on the same temperature scale	Page 38
Figure 26. Temperature dependent functions of $G'$ and $G''$ for a gelling material	Page 40
Figure 27. Complex viscosity, $G'$ , and $G''$ as a function of temperature for an epoxy	Page 40
Figure 28. A gelled 20.0% Soluplus <sup>®</sup> solution on the plate of a cone-and-plate rheometer	Page 41
Figure 29. Sol-gel and gel-sol transitions for Soluplus <sup>®</sup> samples	Page 43
Figure 30. Cloud points for aqueous Soluplus <sup>®</sup> solutions as a function of temperature	Page 44
Figure 31. Log-linear plot of viscosity vs. temperature of aqueous Soluplus <sup>®</sup> solutions at different concentrations	Page 45
Figure 32. Full range of experimental data modeled with a Poly55-Bisquare fit	Page 45
Figure 33. Short range of experimental data modeled with a Poly54 fit	Page 46
Figure 34. Effect of temperature on refractive index for Soluplus <sup>®</sup> samples	Page 48
Figure 35. Effect of temperature on effective diameter for Soluplus <sup>®</sup> solutions using uncorrected values of viscosity and refractive index	Page 50
Figure 36. Effect of temperature on effective diameter for Soluplus <sup>®</sup> solutions using corrected values of viscosity and refractive index	Page 51
Figure 37. Uncorrected vs. corrected diameter at 25.0 °C for Soluplus <sup>®</sup> in solution	Page 51
Figure 38. Size distribution for a 0.1% Soluplus <sup>®</sup> solution at 20.0 °C	Page 53
Figure 39. Viscosity and corrected diameter vs. temperature for 5.0% Soluplus <sup>®</sup> sample	Page 54

## CHAPTER 1. INTRODUCTION

### 1.1 Poor Solubility in the Pharmaceutical Field

In 2011, it was reported that 90% of all compounds in the pharmaceutical drug delivery system were poorly soluble in water.<sup>1</sup> This is a significant problem in the pharmaceutical industry as drugs are ineffective unless they can be solubilized into the body's systems, rather than being excreted from the digestive track due to re-crystallization.<sup>1</sup> It is important that drugs are delivered to the right area, at the right time and at the right concentration, but many obstacles, such as poor solubility, environmental degradation, toxicity, and lack of permeability make drug delivery challenging.<sup>2</sup> These issues have led to the increasing use of enhanced drug delivery methods, such as polymeric micelles, to help drugs reach their molecular target within the body.

### 1.2 Polymers

Polymers are a type of synthetic macromolecule that consist of repeating structural units. They consist of two main components: a backbone and peripheral side chains. The repeating units of a polymer may fall onto either part of a polymer's structure. When a polymer has two or more units of varying composition, it is called a copolymer. Copolymers can be described as random-, alternating-, graft-, or block copolymers. Random copolymers consist of two or more monomers that are simultaneously present in one polymerization reactor. Alternating copolymers are comprised of two different monomers on the structural unit. In graft copolymers, one or more monomers are grafted onto a homopolymer, resulting in a backbone that has perforating side branches. Lastly, in block copolymers one monomer is attached to the end group of a previous

polymerized chain, forming a linear chain with different segments.<sup>3</sup> Table 1 gives visual examples of each type of copolymer along with industrial examples.

Table 1. Types and examples of copolymers.<sup>a</sup>

Type of copolymers	Examples of commercial systems
Alternating copolymers -A-B-A-B-A-B-	Vinylacetate-maleic anhydride-copolymers Condensation polymers of diamines and diacids
Random copolymers -A-A-A-B-A-B-B-A-A-	Styrene-butadiene rubber Styrene-acrylonitrile rubber Ethylene-vinyl acetate copolymer
Graft copolymers A   A   A   -B-B-B-B-B-B-B-B-   A   A   A	Rubber-styrene graft copolymers (high-impact polystyrene)           Acrylonitrile-butadiene-styrene graft copolymer (ABS)
Block copolymers -A-A-A-A-A-A-B-B-B-	Styrene-butadiene diblock copolymers Styrene-butadiene-styrene triblock copolymers Polyurethane multiblock copolymers (elastomeric yarns)

<sup>a</sup> Reproduced from Ref. 3

**1.2.1 Polymer Behavior.** Polymer properties are identified by the polymer's chemical structure and molecular weight distribution. Structure identities such as repeating unit nature, end group nature, and branch composition all effect how a polymer behaves.<sup>3</sup> Block copolymers consisting of unlike chains exhibit complicated physical properties, such as microphase separation that is dependent on polymer length, composition, and concentration.<sup>4</sup> Microphase separation is seen in gelation polymers where a self-assembling of polymer networks causes the polymer to behave as a viscoelastic solid. The polymer gel is soft and deformable, but can hold

its shape, making it of interest in drug delivery science.<sup>5</sup> The gelling of polymers by phase separation is dependent on many conditions, but crucially temperature, giving rise to the terms thermoresponsivity and thermoreversibility, as further discussed in Section 1.3.

Polymers that consist of amphiphilic monomers have the tendency to form micelles in solution. Micelles are colloidal dispersions of these amphiphilic units that self-assemble due to intermolecular forces between the hydrophobic and hydrophilic regions. Typical surfactant micelles are made up of 50 to 200 monomers and have a spherical diameter of three to six nanometers. Polymeric surfactant molecules have spherical diameters that range from 10 to 100 nm.<sup>6</sup> Factors controlling polymeric micelle size include molecular weight of the amphiphilic block copolymer, aggregation number, proportion of hydrophobic to hydrophilic chains, and quantity of solvent trapped inside the micellar core. The driving force behind the self-assembling of polymers into micelles is noted as hydrophobic forces, where the water repelling regions of the polymer aggregate to each other, minimizing the contact between the insoluble block and the solvent, and lowering the free energy of system.<sup>1,6,7</sup> The concentration above which micelles are formed in solution is called the critical micelle concentration (CMC). When at the CMC, or slightly above, loosely aggregated micelles are formed containing solvent within their core. At higher concentrations, the residual solvent is excluded from the core, thereby compacting the micellar structure. In general, polymeric micelles have a lower CMC value than traditional micelles.<sup>6</sup> Many studies show how polymeric micelles can be used in the biomedical field as drug carrier systems.<sup>2,7-11</sup>

**1.2.2 Function with Active Pharmaceutical Ingredients.** Polymeric micelles are capable of encapsulating insoluble active pharmaceutical ingredients (APIs) within their hydrophobic core (Figure 1).<sup>1</sup> Polymeric micelles help to increase the bioavailability of poorly

soluble APIs by stabilizing the drug and keeping it dissolved in solution until it is absorbed in the gastrointestinal track.<sup>12</sup> Surfactants are also used to increase the bioavailability of APIs through topical skin application. The stratum corneum contains a tough barrier in which poorly soluble drugs have trouble penetrating. Encapsulating an API within a polymeric micelle allows for the drug to penetrate the skin as the micelle endures a change in structure due to water evaporation.<sup>10</sup>

Local diseases, e.g. infections or inflammations, are commonly treated by topical delivery of the required medicinal drug to the targeted tissue. It is important that the drug remains at the site of application for an extended time to ensure efficacy and interaction with the disease. Such topical drug formulations require knowledge on rheological properties, such as structure and flow, to gain insight into their effects on drug diffusion and to ensure ease of application/administration. The rheological behavior of polymeric micelles is of increasing interest to test the performance of surfactants in pharmaceutical systems.<sup>9</sup>

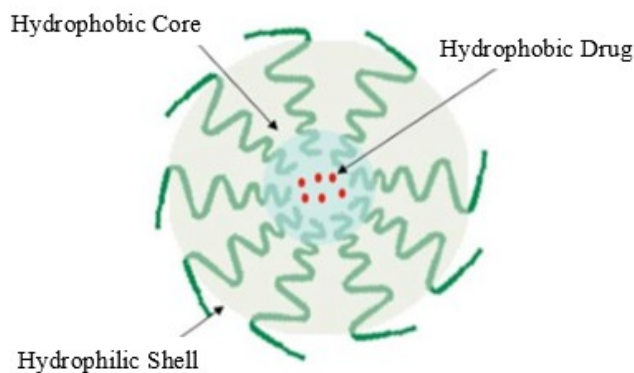


Figure 1. Structure of a polymeric micelle with APIs stored in its core (reproduced from Ref. 8).

### 1.3 Thermoresponsivity

Materials that respond to external stimuli are referred to as “smart materials”. Polymers are the most common smart material because they are comparatively cheap and can respond to

pH, temperature, ionic strength, electric and magnetic fields, and biochemical processes.<sup>2</sup>

Temperature responsive, also referred to as thermoresponsive, polymers are particularly versatile in their applications, such as tissue engineering, sensing, gene delivery and drug delivery.<sup>2</sup> A thermoresponsive polymer's ability to change abruptly and reversibly between various physical states over a range of temperatures gives it elevated interest in the biomedical field.<sup>13</sup>

There are two main types of thermoresponsive polymers in aqueous solutions. The first exhibits a lower critical solution temperature (LCST) in which there is a phase separation upon heating due to the loss of hydration in the system.<sup>13</sup> This phase separation leaves the polymer insoluble at temperatures above the phase boundary, where the boundary is dependent on concentration. The concentration at which the phase separation occurs at the lowest temperature is the LCST.<sup>14</sup> The other type of thermoresponsive polymer exhibits an upper critical solution temperature (UCST) where there is phase separation upon cooling, which is far less common for aqueous polymer solutions (Figure 2).<sup>13</sup> For example, a LCST behaving polymer solution that is below the phase boundary is clear and homogenous, whereas above the transition temperature it appears cloudy.<sup>2</sup> This behavior occurs due to the loss of entropically unfavorable hydrophobic segments at the critical temperature.<sup>13</sup> Considering the Gibbs equation (Equation 1),

$$\Delta G = \Delta H - T\Delta S \quad (1)$$

where  $G$  is Gibbs free energy,  $H$  is enthalpy,  $T$  is temperature, and  $S$  is entropy, the driving force behind phase separation is the entropy of water. When temperature increases and the polymer is not in solution, the water is less ordered and has a higher entropy ( $\Delta S$ ).<sup>2</sup> This decreases the free energy of the system ( $\Delta G$ ), making it more favorable.<sup>2</sup> Polymer solutions that have a UCST are cloudy below the phase boundary but, an increase in temperature, to above the transition state, renders them clear and homogenous. Phase separation of UCST behaving polymer is

enthalpically driven because strongly attractive polymer-polymer interactions are broken by water when the  $T\Delta S$  term outweighs these enthalpic attractions ( $\Delta H$ ).<sup>13</sup>

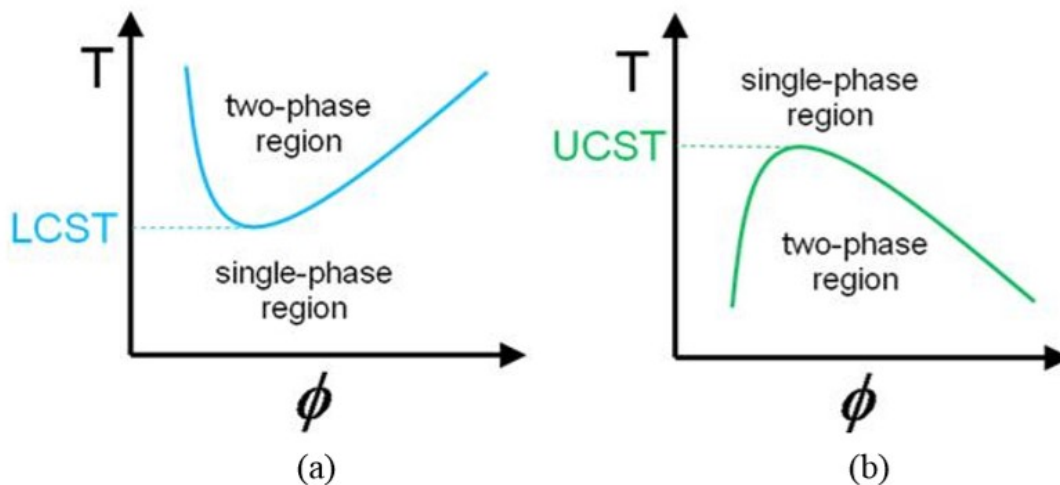


Figure 2. Temperature vs. polymer volume fraction ( $\phi$ ) plots used to illustrate polymer solution phase diagrams for (a) lower critical solution temperature (LCST) behavior and (b) upper critical solution temperature (UCST) behavior (reproduced from Ref. 2).

When LCST and UCST behaving polymers fall within the two-phase region, they de-mix from aqueous solution where the polymer collapses into a globule and forms a precipitate.<sup>15</sup> The temperature at which this transition occurs is referred to as the cloud point and can be witnessed along the phase boundary.

Thermoresponsive polymers may also show properties of gelation, where polymeric micelles self-assemble into lattices at a specified temperature. At this transition temperature, referred to as a sol-gel point, the aqueous solution aggregates and forms a gel. By definition from IUPAC, a gel contains covalently bound polymer networks formed from the crosslinking and physical aggregation of polymer chains.<sup>16</sup> The sol-gel transition is characterized by a large increase in viscosity between the micelle and macrolattice states. Figure 3 shows the molecular

dispersion-to-micelle-to-macrolattice transition at high and low concentrations, where low polymer concentrated solutions don't form macrolattices.<sup>4</sup>

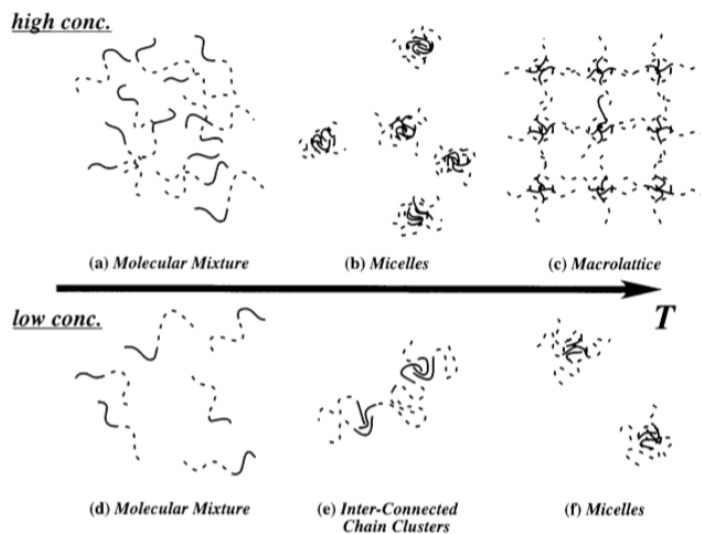


Figure 3. Schematic representation of block copolymer phase transitions at high and low concentrations (reproduced from Ref. 4).

The resulting swollen macrolattice network can also be thermoreversible, in which the regions of local order are thermally reversible.<sup>16</sup> In simpler terms, a thermoreversible polymer will convert back to its original phase after being subjected to a temperature that causes a phase change. For example, a LCST behaving polymer that clouds above the phase boundary will regain transparency when cooled to temperatures below the boundary. This property is important in characterizing how a micelle loaded with APIs will behave once injected into the body.

#### 1.4 Soluplus<sup>®</sup>

Soluplus<sup>®</sup> is a polyvinyl caprolactam-polyvinyl acetate-polyethylene glycol graft copolymer with a respective unit ration of 57:30:13. It was developed by BASF to increase the bioavailability of poorly soluble drugs by making them available in a dissolved state.<sup>17,18</sup> As supplied, Soluplus<sup>®</sup> is a granular substance (Figure 4) with an average molar mass of 118,000



g/mol and a mean grain size of 340  $\mu\text{m}$ .<sup>18</sup> This tri-block amphiphilic copolymer is essentially miscible in water and forms polymeric micelles with a detectable CMC of 7.6 mg/L at 23.0  $^{\circ}\text{C}$ .<sup>18</sup> Figure 5 displays the structure of Soluplus<sup>®</sup> and identifies the hydrophilic and hydrophobic regions that attract to each other to form polymeric micelles. Soluplus<sup>®</sup> dissolves readily at colder temperatures and the solutions exhibit an increase in viscosity as concentration increases.



Figure 4. Physical appearance of Soluplus<sup>®</sup> (reproduced from Ref. 17).

BASF has conducted studies on the solubilization capacity of various APIs when using Soluplus<sup>®</sup> and other well-known surfactants.<sup>19</sup> As seen in Figure 6, Soluplus<sup>®</sup> increased the saturation solubility of several APIs. Soluplus<sup>®</sup> was also able to compete with and in some cases outperform other well-known surfactants. BASF has also reported dissolution tests showing a faster release of a poorly soluble API, itraconazole, in solutions prepared with Soluplus<sup>®</sup> as compared to solutions with other polymeric matrices (Figure 7). As well, they performed bioavailability screenings that showed considerable improvement in the bioavailability of itraconazole in solutions prepared with Soluplus<sup>®</sup> (Figure 8).<sup>19</sup> As suggested in Figures 7 and 8, Soluplus<sup>®</sup> works as a polymeric matrix to improve the amount of administered API dosage that

reaches the bloodstream, overall increasing pharmacokinetic parameters such as drug absorption and distribution.<sup>20</sup>

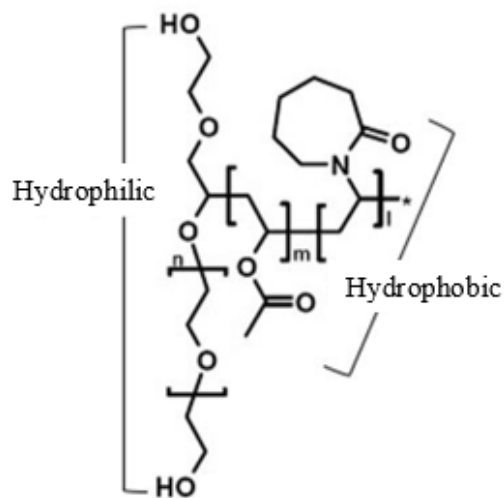


Figure 5. Structure of Soluplus<sup>®</sup>. In the diagram, the indices l, m, and n correspond to the number of units of polyvinyl caprolactam, polyvinyl acetate, and polyethylene glycol respectively (adapted from Ref. 17).

Soluplus<sup>®</sup> is known for its biocompatibility, as documented and marked through toxicological studies presented by BASF. Tested according to OECD (Organization for Economic Cooperation and Development) guidelines, there were no elicited effects from acute toxicity, irritation, or sensitization. The surfactant is not yet listed in the FDA's Inactive Ingredients Database indicating that it has not yet been approved for medicinal use within the US.<sup>15</sup> However, the United States, Germany, France, Japan, and other countries are in clinical trials, with Taiwan and Argentina having already approved Soluplus<sup>®</sup> for use in healthcare products.<sup>15,21</sup>

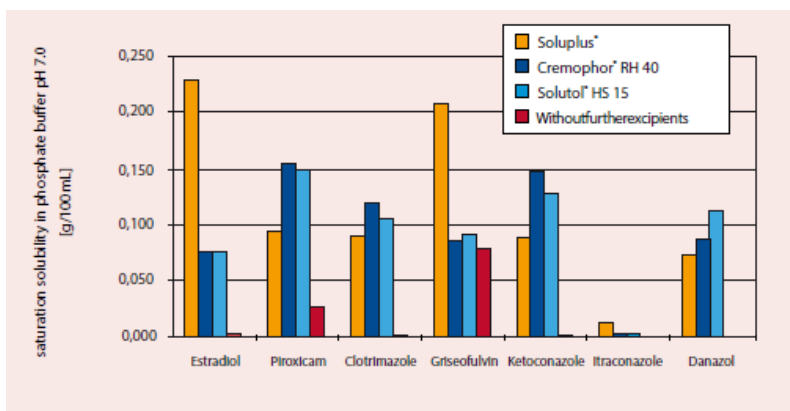


Figure 6. Solubilization capacities of various active pharmaceutical ingredients with and without solubilizing excipients (reproduced from Ref. 19).

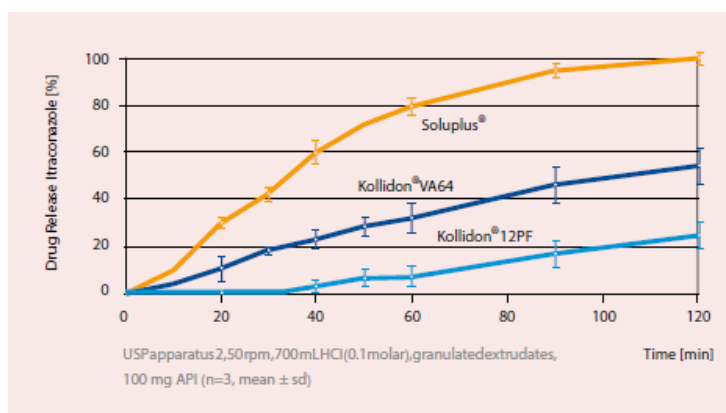


Figure 7. Dissolution test for the release of itraconazole with various polymeric matrices (reproduced from Ref. 19).

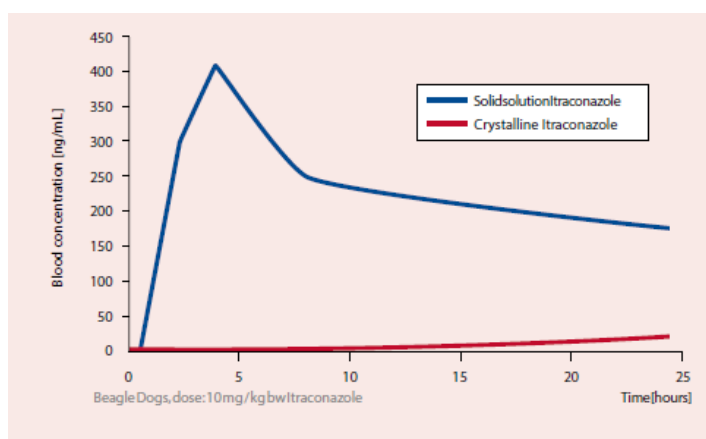


Figure 8. Blood concentration of itraconazole with and without Soluplus<sup>®</sup> solution (reproduced from Ref. 19).

Solutions of Soluplus<sup>®</sup> show an increase in viscosity upon warming, referred to as thermothickening, which is a property of potential interest in topical drug applications. A thermothickening solution can flow through an applicator/syringe but then may harden as it makes its way into the body.<sup>15</sup> This makes it possible to mix APIs with a polymer in its liquid room-temperature state, but then witness an *in-situ* gel deposit at the injection site when the polymer is at body temperature.<sup>22</sup> The polymers, polyvinyl caprolactam and polyethylene glycol are known to transition from a hydrophilic to amphiphilic state upon warming, around 34 °C to 36 °C, which results in the self-assembly of micelles and gelation.<sup>15</sup> Because Soluplus<sup>®</sup> is comprised of these components it is suspected that a similar mechanism occurs upon heating of aqueous solutions of Soluplus<sup>®</sup>.<sup>15</sup> Soluplus<sup>®</sup> also exhibits a gel-sol transition phase as temperatures continue to rise.<sup>23</sup> This unusual physical behavior is seen only in doubly thermoresponsive polymers that exhibit both LCST and UCST behavior. Specifically, Soluplus<sup>®</sup> is a LCST < UCST behaving polymer and forms a gel within a designated temperature range. Copolymers that contain OH-functionality, e.g. polyvinyl acetate, polyethylene glycol, polyvinyl butyrate, and protonated acrylic acid, generally show LCST < UCST behavior, rather than UCST < LCST.<sup>13</sup> As seen in Figure 9, the circular temperature-concentration phase diagram describes how Soluplus<sup>®</sup> transitions from a soluble to insoluble phase, and then back to a soluble phase as a function of increasing temperature.<sup>13</sup>

Soluplus<sup>®</sup> forms micelles in aqueous media, where the hydrophobic regions, polyvinyl acetate and polyvinyl caprolactam, are located in the core of the micelle and the hydrated polyethylene glycol segment is located in the outer region.<sup>7,18</sup> The micellization of Soluplus<sup>®</sup> in water is known to be endothermic and is spontaneous at temperatures above the Krafft point (critical micelle temperature) due to an entropically-driven Gibbs free energy. During

micellization, solvent is released and entropy increases. This gain in entropy exceeds the loss of entropy by self-assembly of the polymeric micelles, leaving the system with a positive entropy change. The micellization process occurs in three steps: 1) polymeric micelles are formed in solution at concentrations and temperatures above the CMC and Krafft point, 2) the polyethylene glycol chains dehydrate at temperatures above the Krafft point but below the phase boundary, and 3) there is an onset of physical change as temperature increases (Figure 10).<sup>7</sup> This change could be a cloud point, where precipitation from solution at the LCST phase boundary causes opacity, or the change could be gelling due to self-assembly and aggregation of micelles into an entangled network at a temperature specified as the sol-gel point. A thermoresponsive polymer may exhibit both physicochemical changes, clouding and gelling, however, based on previous work in our research group, these physical onsets do not show any correlation, other than their dependence on increasing temperatures.<sup>24</sup> The micellization process is dependent on temperature, polymer concentration, and medium composition.<sup>7</sup>

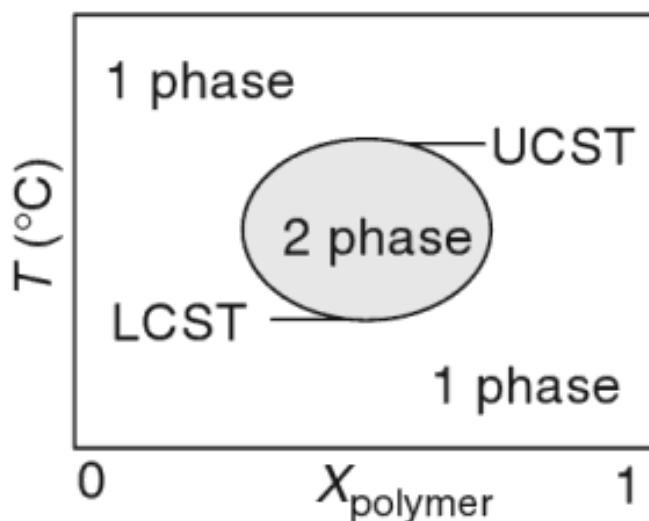


Figure 9. Phase diagram for a  $\text{LCST} < \text{UCST}$  behaving polymer (reproduced from Ref. 14).

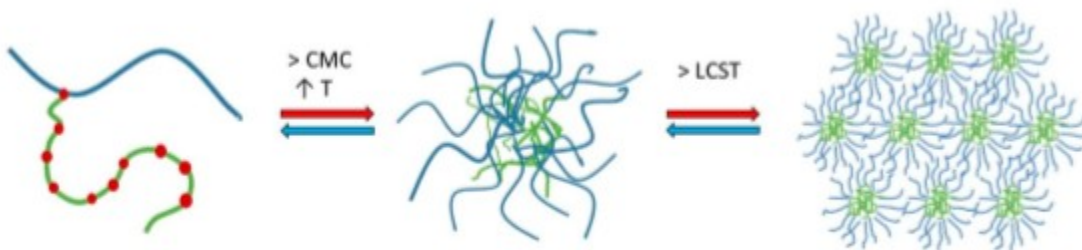


Figure 10. Micellization mechanism for solutions of Soluplus<sup>®</sup> (reproduced from Ref. 7).

As Soluplus<sup>®</sup> solutions, below 30.0% (w/w), proceed through the micellization process they encounter a series of temperature dependent physical behaviors. At temperatures below the LCST phase boundary, Soluplus<sup>®</sup> solutions appear clear with unrestricted flow. At temperatures above the boundary, the solution clouds before a further increase in temperature causes a sol-gel transition and restricted flow (Figure 11).<sup>22</sup> Soluplus<sup>®</sup> solutions above 30.0% (w/w) show restricted flow at room temperature, but remain clear.<sup>24</sup> This indicates that the solutions have not crossed the LCST phase boundary into the clouding region, but have undergone a sol-gel transition. It is suggested that gelling can occur when polymer concentration is substantially large.<sup>7</sup>



Figure 11. A 30.0% (w/w) Soluplus<sup>®</sup> solution at room temperature (left), cloud point (middle) and gel point (right). Represented as a top view of the cone-and-plate rheometer sample compartment that was lowered from its housing and subjected to increasing temperatures.

## 1.5 Dynamic Light Scattering Spectroscopy

An important characteristic of solubility enhancers is their particle size in solution before and after loading with APIs. Polymeric micelle particle size is studied through dynamic light scattering spectroscopy (DLS). This technique, also known as photon correlation spectroscopy or quasi-elastic light scattering, measures the translational diffusion of macromolecules in solution due to Brownian motion.<sup>25</sup> Brownian motion refers to the random scattering of particles due to collisions with solvent molecules. Larger molecules have a slower Brownian motion, while smaller particles are bombarded further by surrounding solvent molecules and have more rapid movement.<sup>26</sup> The Stokes-Einstein equation is used in dynamic light scattering methods to relate the diffusion coefficient to particle size.<sup>27</sup> Equation 2 defines the Stokes-Einstein equation,

$$d(H) = \frac{kT}{3\pi\eta D} \quad (2)$$

where  $d(H)$  is hydrodynamic diameter,  $k$  is Boltzmann's constant,  $T$  is absolute temperature,  $\eta$  is viscosity of solvent, and  $D$  is the velocity of Brownian motion, typically defined as the translational diffusion coefficient.<sup>26</sup>

**1.5.1 Effect of Viscosity.** As seen in Equation 2, particle size measurements by DLS are dependent on temperature and the viscosity of solvent. This dependence is seen in calculations and in how the sample behaves. Particles can behave in Newtonian or non-Newtonian manner. Newtonian fluids refer to samples that have the same viscosity at constant temperature and pressure, regardless of the amount of stress and shear strain.<sup>27</sup> For example, a Newtonian fluid would move twice as fast if it were subjected to twice as much force.<sup>28</sup> In a non-Newtonian fluid, the particles are suppressed by a larger viscosity of solution, therefore restricted from Brownian motion. Viscosities of greater than three centipoise (cP) are generally considered as non-

Newtonian. Results from DLS measurements can be significantly affected by inaccurate viscosity values.<sup>27</sup>

As seen in Figure 12, the analysis of a pigment dispersed in water was altered by using different viscosities. The blue graph was analyzed using a viscosity of 1.0 cP in the sizing algorithm and the red graph was recomputed using 2.0 cP. A particle size shift from 700 nm to 350 nm shows just how dependent hydrodynamic diameter measurements are on viscosity.<sup>27</sup> Particle size is also affected by particle concentration, ionic strength of medium, surface structure, particle shape, and the refractive index of solvent.<sup>26,27</sup>

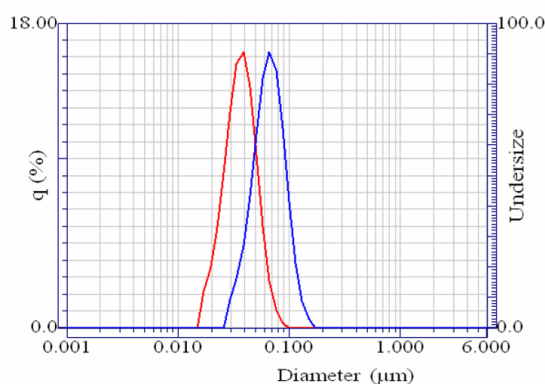


Figure 12. Particle size data for a pigment dispersed in water at two different viscosities: 1.0 cP (blue) and 2.0 cP (red) (reproduced from Ref. 27).

A Further Look into Rheology. Rheology is the study of deformation and flow, branching from the physical sciences which study the mechanics of forces, deflections, and velocities.<sup>29</sup> Newton was one of the first philosophers to investigate the quantification of a fluid's viscosity. He originally described viscosity as the lack of “slipperiness” between elements of a fluid as they are forced to move past each other. Rheology has advanced throughout the ages from testing viscosity by dropping heavy spheres through material and recording time differences, to using advanced and accurate instrumentation.<sup>30</sup> Rheology is observed in everyday life through liquids



and solids such as honey, gum eraser, toothpaste, syrup, oil, rubber and much more. These materials behave simultaneously in a fluid (viscous) and solid (elastic) way, giving rise to the term viscoelasticity. Rheology studies the deformation of viscoelastic materials when subjected to a shear force that causes the material to flow.<sup>29</sup>

Purpose of Studying Flow and Deformation. Flow behavior is studied to pre-emptively design equipment and practice quality control.<sup>28</sup> Various industries provide great examples of using these studies in testing their products. Ketchup must flow out of the bottle when shaken or squeezed. Household paint is easily stirred but dries on a wall without dripping. Pudding seems solid at rest, but is simply spooned from the cup, and ointment must effortlessly squeeze from the tube with moderate pressure.<sup>28,31</sup> The pressure at which a fluid just begins to flow, a fundamental quality control concern, is known as the yield stress.<sup>28</sup> Yield stress measurements can be routinely performed by using viscometers and rheometers, later discussed in Section 2.3.1.

Flow and deformation are also studied to characterize a material. Viscosity is a “window” into other properties of a material that may be harder to measure. When analyzing a sample for its viscosity, information is also gained regarding temperature, shear rate, time, pressure, and material composition. It is important to know how a product will react when subjected to these other conditions. For example, motor oils and greases will have a decrease in viscosity when subjected to higher temperatures.<sup>28</sup> As well, lubricating oils decrease in viscosity at high temperatures which cause the oils to flow off the metal parts they protect.<sup>32</sup> Shear rate, or the rate of deformation, can also impact a sample, causing a material to change in viscosity during various times in the production process.<sup>28</sup> Many materials also undergo changes in viscosity during a chemical process or while subjected to an outside pressure, making rheological measurements dependent on time and pressure. Lastly, a materials composition can affect

viscosity. The state of aggregation between the solid particles and liquid phase, in emulsions and dispersions, causes viscosity differences due to clumping and packing shape. This is seen in milk, which is emulsified fat globules within water.<sup>28</sup>

Viscosity, Shear Stress, and Shear Rate. Rheology describes the elasticity, viscosity, and plasticity of materials. The interest is specifically on viscosity and the following parameters that accompany it: shear stress and shear rate.<sup>28</sup> Viscosity is defined as the measure of the internal friction of a fluid. This implies that one layer of fluid passes another layer without a transfer of matter, called laminar flow (Figure 13). A greater amount of friction between the layers corresponds to a greater amount of force required for the movement.<sup>28</sup>

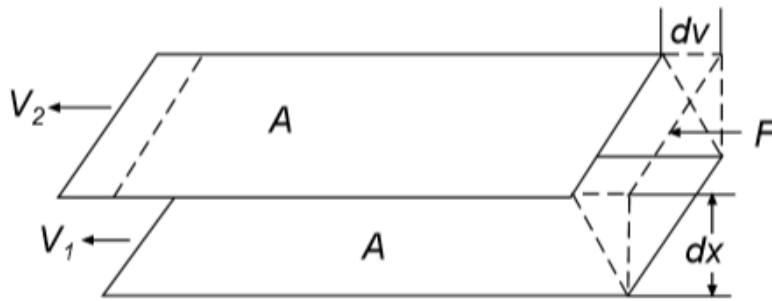


Figure 13. Two plates model used to describe the physics of viscosity, where  $A$  is the area of fluid,  $V_1$  and  $V_2$  are the velocities at which the fluid is moving,  $dv$  is difference in velocities,  $dx$  is the distance between the two fluids, and  $F$  is the force required to cause movement (reproduced from Ref. 28).

As seen in Figure 13, two parallel, flat areas of fluid, separated by a designated distance, are moving in the same direction at varied speed. From this model, Newton implied that the force needed to maintain the difference in speeds was proportional to the difference of speed through the liquid. This velocity gradient ( $\frac{dv}{dx}$ ) is expressed by Equation 3,

$$\frac{F}{A} = \eta \frac{dv}{dx} \quad (3)$$

where  $\eta$  is a given material's constant known as viscosity.<sup>28</sup> The velocity gradient describes the shearing a liquid experiences and is thus known as the shear rate, or rate of deformation. The force per unit area ( $\frac{F}{A}$ ) term represents the shear stress, or what is causing the shearing action.

Equation 4 defines viscosity using these terms,

$$\eta = \frac{\tau}{\dot{\gamma}} \quad (4)$$

where  $\tau$  is shear stress and  $\dot{\gamma}$  is shear rate.<sup>28</sup> Shear stress has a unit of Newtons per square meter ( $\text{N/m}^2$ ) and shear rate is in units of reciprocal seconds ( $\text{sec}^{-1}$ ). Viscosity has a fundamental unit of “poise”, where a material requiring one  $\text{N/m}^2$  of shear stress to produce a shear rate of one  $\text{sec}^{-1}$  has a viscosity of one poise. Viscosity measurements are typically written on the centipoise scale (cP). Measurements may also be seen in mPa·s (millipascal-seconds) which have a 1:1 ratio with cP.<sup>28</sup> Table 2 gives common viscosities of many household goods.

Table 2. Approximate viscosity values of commonly known materials at 20.0 °C.<sup>b</sup>

Fluid	Viscosity (cP)
Water	1
Milk	3
Olive Oil	80
Glycerin	1,000
Honey	10,000
Toothpaste	70,000
Peanut Butter	250,000

<sup>b</sup> Adapted from Ref. 33

Viscosity can also be referred to in terms of  $G^*$ , the complex shear modulus, which is equivalent to viscosity,  $\eta$ . The complex shear modulus can be broken down into two components,  $G'$  and  $G''$ , the storage and loss moduli, respectively. The storage modulus,  $G'$ , is responsible for characterizing the elastic behavior in viscoelastic materials, while the loss

modulus,  $G''$ , describes the viscous behavior. Elastic behavior arises when energy is stored within a material that has been subjected to deformation. The internal structures extend and stretch without causing damage to the material, allowing the stored energy to act as a driving force in returning the material back to its original state. Viscous behavior results from internal friction between a materials molecules and particles when subjected to deformation. As friction builds, the material absorbs heat, causing a loss of energy. The storage modulus represents the energy stored from deformation while the loss modulus characterizes the energy dissipated by internal friction. Viscoelastic solids have a higher storage modulus than loss ( $G' > G''$ ) due to their physical-chemical linking, whereas viscoelastic liquids have a greater loss modulus than storage ( $G'' > G'$ ) due to the lack of strong interactions between molecules.<sup>34</sup> Figure 14 describes the relationship between complex shear modulus and phase-shift ( $\delta$ ), which is the lag time between the current and resulting sinusoidal oscillation.<sup>34</sup> The relationship between  $G^*$ ,  $G'$ , and  $G''$  is seen in Equation 5, which follows the Pythagorean theorem.

$$|G^*| = \sqrt{(G')^2 + (G'')^2} \quad (5)$$

Using Equation 5 allows for the determination of  $G^*$ , or viscosity, from  $G'$  and  $G''$ .<sup>29</sup> Another parameter, loss factor, reveals the ratio of viscous to elastic behavior and is calculated as the tangent of the phase-shift angle as seen in Equation 6.<sup>29,34</sup>

$$\tan \delta = \frac{G''}{G'} \quad (6)$$

When the loss factor is greater than one ( $\tan \delta > 1$ ), it signifies the sample is in liquid “sol” state. When the loss factor is less than one ( $\tan \delta < 1$ ), it signifies a solid “gel” state. The “sol-gel” transition state of gelation polymers is seen when the loss factor is equivalent to one ( $\tan \delta = 1$ ).<sup>29</sup>

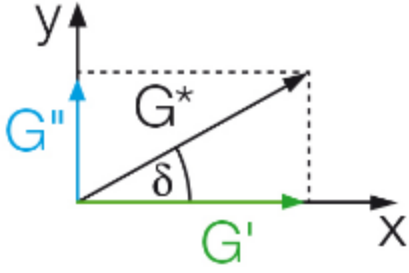


Figure 14. Graphical relationship between complex shear modulus  $G^*$ , storage modulus  $G'$ , loss modulus  $G''$ , and the phase-shift angle  $\delta$  (reproduced from Ref. 34).

**1.5.2 Effect of Refractive Index.** The refractive index of solution medium plays a crucial role in light scattering. Its dependence is seen in the correlation function of a typical DLS measurement, where the intensity of scattered light is transformed into a size distribution by using various algorithms. For most monodisperse particles in Brownian motion, the correlation function ( $G$ ) follows an exponential decay as seen in the Equation 7,

$$G(\tau) = A[1 + B \exp(-2\Gamma\tau)] \quad (7)$$

where  $\tau$  is the correlator time delay,  $A$  and  $B$  are the baseline and intercept of the correlation function respectively, and  $\Gamma$  is further defined in Equation 8,

$$\Gamma = Dq^2 \quad (8)$$

where  $D$  is the translational diffusion coefficient. Refractive index is seen within the definition of  $q$  as follows in Equation 9,

$$q = \left(\frac{4\pi n}{\lambda}\right) \sin\left(\frac{\theta}{2}\right) \quad (9)$$

where  $n$  is refractive index,  $\lambda$  is the wavelength of the laser, and  $\theta$  is the scattering angle.<sup>26</sup>

Refractive index becomes increasingly more important in the correlation function when using a volume distribution display mode that presents the size distribution as a ratio of volume to mass.

Using a volume distribution display mode is practical when the size of particles becomes roughly

equivalent to the wavelength of the excitation light and is known as Mie theory.<sup>25,26</sup> Specifically, Mie theory compares the size of particles to the wavelength of light by considering particle shape and difference in refractive index between particles and the medium they are present in, while utilizing a volume distribution display mode.<sup>25</sup>

## 1.6 Objectives

This project investigates how the viscosity and refractive index of aqueous Soluplus<sup>®</sup> solutions affects polymeric micelle size as determined by DLS. It is hypothesized that if the temperature dependence of viscosity for aqueous Soluplus<sup>®</sup> solutions is rheologically measured and the relationship between concentration, temperature, and viscosity is used in DLS algorithms, then DLS particle size measurements will be more reliable in describing the physical behavior of Soluplus<sup>®</sup>.

The goals of this project include:

1. Analyze the viscoelastic behavior for aqueous Soluplus<sup>®</sup> solutions as a function of temperature and establish a mathematical relationship between concentration, temperature, and viscosity.
2. Evaluate the refractive index of Soluplus<sup>®</sup> solutions as a function of temperature.
3. Compare DLS particle size measurements for aqueous solutions of Soluplus<sup>®</sup>, using the viscosity and refractive index of water versus the viscosity and refractive index of actual solution.

## CHAPTER 2. EXPERIMENTAL

### 2.1 Overview

Soluplus<sup>®</sup> solutions, 1.0% to 30.0% (w/w), were tested on a cone-and-plate rheometer for their temperature dependence of viscosity. The rheometer was set to external mode and controlled through a software interface. A relationship between viscosity, concentration, and temperature was created by fitting a polynomial regression to a 3D plot of these variables. The refractive indices of Soluplus<sup>®</sup> solutions were analyzed as a function of temperature and used, along with viscosity data, to correct inputs within DLS algorithms for particle size analysis on Soluplus<sup>®</sup> solutions ranging 0.1% to 10.0%.

### 2.2 Materials

Soluplus<sup>®</sup> was provided to Missouri State University's Department of Chemistry by BASF Corporation (Ludwigshafen, Germany).<sup>35</sup> Aqueous Soluplus<sup>®</sup> solutions were made ranging from 1.0% to 30.0% (w/w) for *analysis by rheometry*. Using an analytical balance (Mettler Toledo AL104) and deionized water, a 30.0% (w/w) solution of Soluplus<sup>®</sup> was made and then further diluted to other concentrations by weight. The targeted weight of solutions was 15.0 g. This process was repeated twice more, to have a total of three sets of Soluplus<sup>®</sup> solutions (further labeled as Sets 1, 2, and 3). When making aqueous Soluplus<sup>®</sup> solutions, the solid powder is added to the water, briefly stirred, and then refrigerated around 5.0 °C until dissolved.

*For analysis by DLS and refractometry*, Soluplus<sup>®</sup> solutions ranging 0.1% to 10.0% (w/w) were made using an analytical balance (Mettler Toledo AL104), 18 MΩ (Type I) water (Barnsted Nanopure II with 4 Mod Organic Free cartridge kit), and sterilized equipment. Each

solution had a targeted final weight of 60.0 g and was made as described above. However, in these cases the solutions were made individually instead of being diluted from a stock solution. Again, three sets of Soluplus<sup>®</sup> solutions were made and labeled as Sets 1, 2, and 3. It is crucial that sterilized equipment and highly filtered water is used to make the solutions, as DLS is very sensitive to outside contaminants and dust.

## **2.3 Temperature Dependence of Viscosity**

**2.3.1 Instrumentation.** Rheology is quantified through use of viscometers and rheometers. As described in Section 1.5.1, these instruments are used to measure viscosity, shear stress, torque, and shear rate. Rheometers allow for the measurement of rheological behaviors on non-Newtonian fluids and for characterization of flow and deformation.<sup>36</sup> These rheological behaviors include specific property measurements of viscoelasticity, yield stress, and stress relaxation.<sup>37</sup> Rheometers are distinguished into two categories: shear rheometers (sometimes referred to as rotational rheometers) and extensional rheometers. Shear rheometers control shear stress by applying the independent variable of torque, while extensional rheometers control strain and measure stress as the dependent variable.<sup>38</sup> There are three types of shear rheometers, which include capillary, rotational cylinder, and cone-and-plate setups.<sup>39</sup> This research exclusively uses a cone-and-plate rheometer to conduct all viscosity analyses. Cone-and-plate rheometers determine absolute viscosity with precise shear rate and stress information available. They require minimal volume of sample and can control temperature through a jacketed sample cup. This geometry is specifically useful in determining rheological behaviors of non-Newtonian fluids.<sup>28</sup> However, cone-and-plate rheometers are not useful in testing samples that show a three-dimensional structure such as gels and solids. When particles in agglomerate systems become too



large, there isn't enough free space between the particles in motion causing a greater amount of friction on the instrument's surfaces.<sup>29</sup>

The principle of operation behind a rotational rheometer is to drive a spindle through a calibrated beryllium copper spring into viscous solution within the plate. The drag of the sample is measured by spring deflection and translated into torque and viscosity measurements.<sup>31</sup> A greater amount of internal friction requires a greater amount of force needed to move the spring through layers of fluid.<sup>28</sup> As seen in Figure 15, the motor, pivot shaft, spring, and spindle are housed in the upper half of the rheometer. A jacketed cup, containing the sample, is joined to the upper half of the instrument where the spindle rotates at the intersection of these parts. The gap between the cone and plate is crucial for accurate viscosity measurement. It is determined by locating the "hit point" and then backing off the spindle by one scale division (as designated on the instrument). The hit point is where the spindle first comes in contact with the plate, causing the torque to change from 0.0% to 1.0% or greater.<sup>31</sup> The cone angle is also of importance, as it keeps constant torque at all distances from the center of rotation.<sup>40</sup>

At a given viscosity, the degree of resistance on the spring is proportional to the spindle's size, geometry, and speed (Figure 16).<sup>28</sup> Choosing an optimal match of spindle diameter and rotational rate is commonly done by trial and error; however, it is known that viscosity range is inversely proportional to both of these parameters. Therefore, samples with a higher viscosity should be performed with a smaller spindle and/or slower speed. Measurements are recommended to be made within a torque range of 10.0% to 100%.<sup>31</sup>

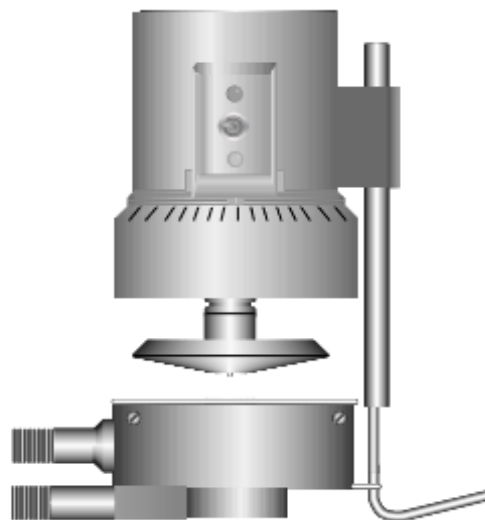


Figure 15. Schematics of a cone-and-plate rheometer (reproduced from Ref. 31).

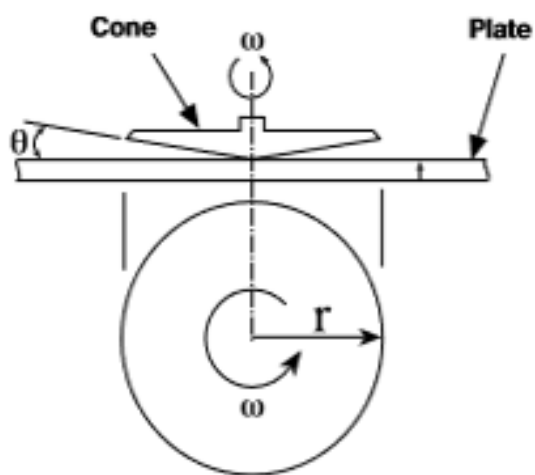


Figure 16. Diagram of the inner workings of the cone and plate where  $\omega$  is the rotational velocity,  $r$  is the cone radius, and  $\theta$  is the cone angle (adapted from Ref. 28).

The rheometer used in this research was a DV-III Ultra programmable rheometer, model RVDV-III, from AMETEK Brookfield (Middleboro, MA, USA). This cone-and-plate rheometer was provided to Missouri State University, Department of Chemistry by Tolmar Inc. (Fort Collins, CO, USA). Calibration was performed by Brookfield in July 2019 to ensure proper

torque readings and drive shaft function. Spindles used for measurement included the CP40 and CP52 (Table 3, Figure 17), allowing for a total viscosity range of 1.31 cP to 9,922,000 cP.

Table 3. Cone spindle dimensions and shear rates.<sup>c</sup>

Cone Spindle	Angle (degrees)	Radius (cm)	Sample Size (mL)	Shear Rate (sec <sup>-1</sup> )	Viscosity Range (cP)
CP-40 / CPA-40Z	0.8	2.4	0.5	7.5N*	1.31 – 327,000
CP-52 / CPA-52Z	3.0	1.2	0.2	2.0N	39.69 – 9,922,000

<sup>c</sup> Adapted from Ref. 28

\*N = RPM



Figure 17. Top view of spindles CP40 (left) and CP52 (right).

The rheometer was controlled through Brookfield's *Rheocalc* software (Ver. 3.3, Brookfield Engineering Laboratories, Inc.) which allows for the programming of conditions and graphical views of viscosity as a function of temperature. In order to obtain temperature measurements through Rheocalc, a probe from Brookfield was adjoined to the instrument. The only appropriate attaching probe was the DVP-94Y steel temperature probe that is used in vane spindle rheometer set ups. The cone-and-plate set up required a temperature probe with a flexible tip, so that the measurement could be taken underneath of the metal sample cup. To account for this problem, the steel DVP-94Y probe was purchased along with a 100 ohm 4-wire resistance

temperature detector (Omega, part # RTD-3-F3105-36-G). The probes were spliced and connected so that the DVP-94Y steel probe connected into the rheometer, but the flexible end of the 4-wire resistance temperature detector attached to the sample cup. This successfully allowed for the transmission of temperature from the instrument into the software. The temperature of samples was controlled using a Fisher Scientific Isotemp Refrigerated Circulator (Model 910) that was connected to the input and output ports of the instrument's sample cup (see Figure 15).

Calibration standards were purchased from Brookfield to confirm the accuracy and precision of the instrument. Two 100% PAO (polyalphaolefin) oil viscosity standards (352.4 cP and 3,439 cP) were tested and showed accuracy according to the specifications defined by Brookfield. These specifications and calibration results can be seen in Section 3.1.

**2.3.2 Methods.** Brookfield calibration standards and Soluplus<sup>®</sup> samples, 1.0, 2.0, 5.0, 10.0, 15.0, 17.5, 20.0, 22.5, 25.0, and 30.0 % (w/w), were evaluated through use of the Brookfield DV-III Ultra programmable rheometer and the software, Rheocalc, for their temperature dependence of viscosity. Each sample/standard was evaluated from 5.0 °C to about 40 °C at a heating rate of 0.1 °C/sec. A sample volume of 0.5 mL was placed into the cup of the rheometer and probed with the specified spindle and shear rate (Table 4). All programming parameters were set in Rheocalc and the experimental set-up was as shown in Figure 18. Data were collected at a rate of one point per second, while the total collection time was set to one hour. The resulting data were exported to Microsoft Excel (Ver. 2002) for plotting and further analysis. The process was run in triplicate for the purpose of determining and reporting uncertainties.

Table 4. Experimental conditions for each sample/standard run on the rheometer.

Soluplus® (%)	Spindle	RPM
352.4 cP Std.	CP40	2.00
3.439 cP Std.	CP52	10.0
1.0	CP40	250
2.0	CP40	250
5.0	CP40	250
10.0	CP40	75.0
15.0	CP40	20.0
17.5	CP52	250
20.0	CP52	250
22.5	CP52	100
25.0	CP52	15.0
30.0	CP52	1.00

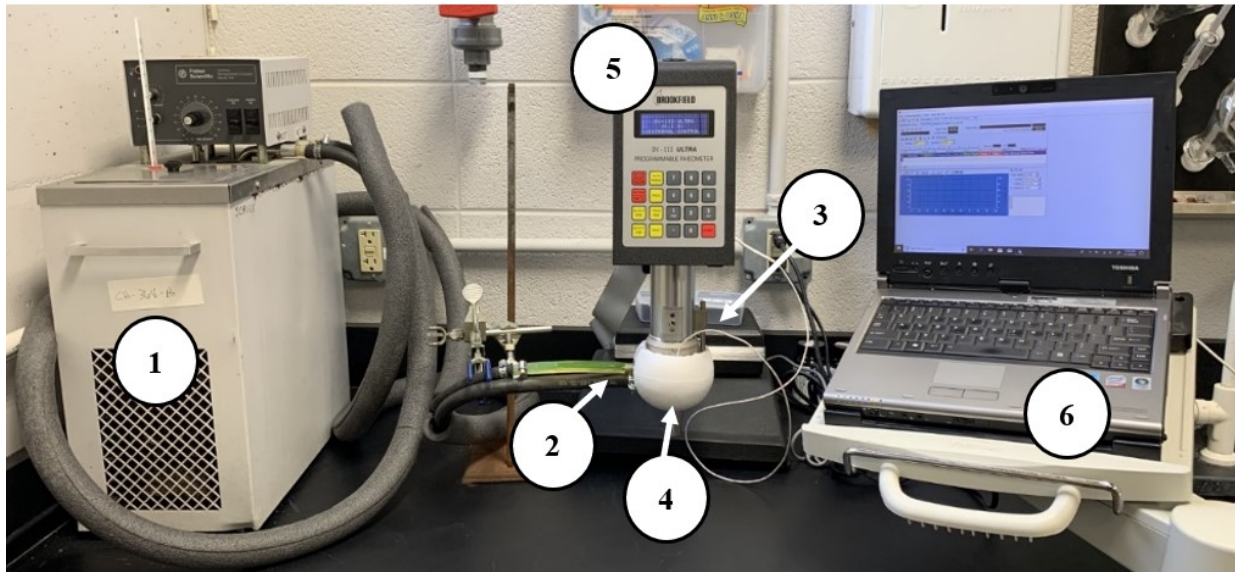


Figure 18. Set-up used for viscosity data collection on a Brookfield rheometer. A refrigerated circulator (1) was connected to the rheometer’s sample cup ports (2) for temperature control. A RTD probe (3) attached to the cup was used to measure temperature, where a Styrofoam cap (4) was used to insulate the sample cup. The rheometer (5) was externally connected to a laptop (6) with the software, Rheocalc.

## 2.4 Refractive Index Analysis

**2.4.1 Instrumentation.** Refractive index was measured using a 2WJ monocular Abbe-type refractometer (Figure 19) that was set up to allow for temperature control over a range of

0.0 °C to 70.0 °C. The instrument has an index range of 1.3 to 1.7 with an accuracy of  $\pm 0.0002$ . Water and ethanol were used as calibration standards ( $n = 1.3330$  and  $1.3611$  at 20.0 °C respectively) to test the accuracy of the instrument. The results of all refractive index measurements are presented in Section 3.2.

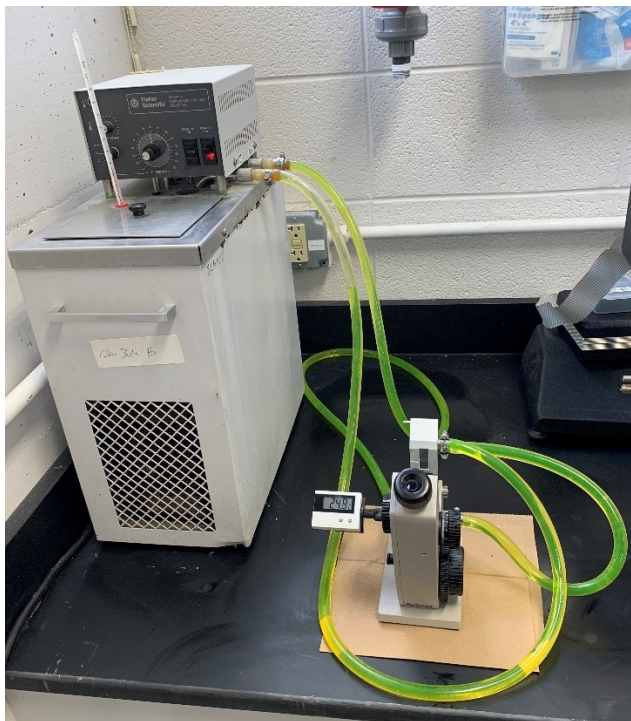


Figure 19. Set-up used for refractive index data collection on an Abbe refractometer.

**2.4.2 Methods.** Water, ethanol, and Soluplus<sup>®</sup> samples (0.1, 0.5, 1.0, 2.0, 5.0, and 10.0%) were evaluated using the 2WJ Abbe digital refractometer for their refractive index following the temperatures defined in Table 5. For each sample, the refrigerated circulator was first set to the appropriate temperature, then a few drops of sample were placed between the measuring prisms, and lastly the dispersion correction and adjustment knobs were fine-tuned to where the shadow aligned with the crosshairs, giving a refractive index reading (Figure 20). To evaluate the aqueous Soluplus<sup>®</sup> samples from 11.0 °C to 35.0 °C, the circulator was cooled to the starting

temperature and slowly ramped to the final temperature, where refractive index readings were taken every 1.0 °C. The 0.1% Soluplus<sup>®</sup> sample was evaluated in triplicate for the purpose of determining and reporting uncertainty.

Table 5. Temperatures used in the evaluation of refractive index for various standards and samples.

Soluplus <sup>®</sup> (%)	Temperature (°C)
Water (Std.)	20.0
Ethanol (Std.)	20.0
0.1	11.0 - 35.0
0.5	11.0 - 35.0
1.0	11.0 - 35.0
2.0	11.0 - 35.0
5.0	11.0 - 35.0
10.0	11.0 - 35.0

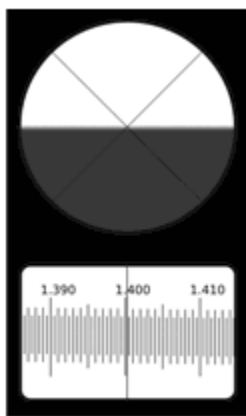


Figure 20. Shadow and scale within an Abbe-type refractometer. A sample's refractive index (bottom) is defined as the position where the shadow aligns with the crosshairs (top) (reproduced from Ref. 41).

## 2.5 Particle Size Determination by Dynamic Light Scattering

**2.5.1 Instrumentation.** The velocity of translational diffusion due to Brownian motion is measured in DLS by using a monochromatic beam of light which causes the scattering of light

upon interaction with molecules. When the incident light encounters a molecule, it is scattered in all directions based on the size and shape of particle. The scattered light will either result in mutually destructive phases, canceling out, or in constructive phases, producing a detectable signal.<sup>25</sup> A digital autocorrelator then correlates intensity fluctuations of scattered light to time. This determines the rate at which intensity fluctuates, which is related to the diffusion of molecules. In dynamic light scattering, the intensity correlation function is measured and expressed as hydrodynamic diameter data.<sup>25,26</sup> Figure 21 gives a representative scheme of the working parts in a DLS instrument.

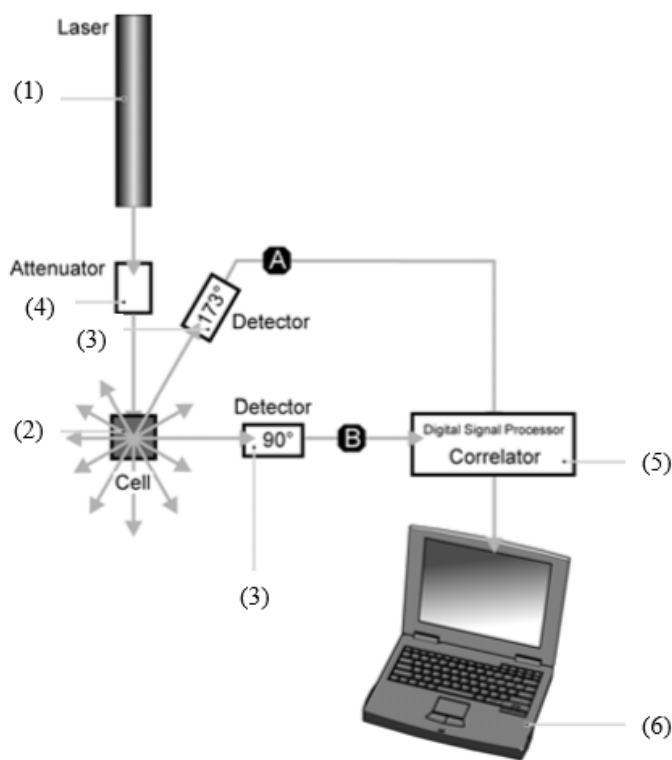


Figure 21. Schematic representation of the Zetasizer Nano series DLS instrument including a laser (1), sample cell (2), detector (3), attenuator (4), correlator (5), and computer source (6) (adapted from Ref. 26).



There are 6 components to a DLS system. As labeled in Figure 21, the first component is a laser (1) that provides a light source to illuminate the sample cell (2). Next, a detector (3) is either placed at  $90^\circ$  or  $173^\circ$  to collect the scattered light. If too much light is reaching the detector, the attenuator (4) will reduce the intensity of the light source. Conversely, if not enough light is being detected, the attenuator will allow more light to reach the sample. Once the detector senses the scattered light intensity, it sends the data to the correlator (5) which translates the rate of light intensity fluctuation. Finally, a computer (6) analyzes the data through software and derives size information.<sup>26</sup>

There are many advantages to using DLS as a particle size measurement technique. These include having a wide range of sample temperature and concentration parameters and being a non-invasive, low sample volume requirement technique. Some limitations to DLS include low resolution, tedious cleaning and filtering procedures, time-consuming optimization of parameters, restriction to transparent samples, and most importantly for this research, the sensitivity to temperature, solvent viscosity, and refractive index.<sup>25</sup>

Research was conducted using a Brookhaven (Holtsville, NY, USA) NanoBrook Omni particle size and zeta potential analyzer (Figure 22). This instrument utilized dynamic light scattering techniques with a 40 mW 640 nm red laser and collection angles of  $15^\circ$ ,  $90^\circ$  and  $173^\circ$ . The measurement range is 0.3 nm to 10  $\mu\text{m}$  with temperature control from  $-5.0^\circ\text{C}$  to  $110^\circ\text{C}$ . Data collection was accomplished by using Brookhaven Instrument's Particle Solutions software (v.3.6.0.6376), which allowed for the programming of experimental conditions and for data viewing/manipulation.

NIST (Gaithersburg, MD, USA) latex calibration standards were used to ensure accurate performance of the DLS. Two standards, 40 nm and 300 nm, were tested and showed accurate results according to the manufacturer's specifications (see Section 3.2).<sup>42</sup>



Figure 22. Set-up used for particle size data collection on a NanoBrook Omni.

**2.5.2 Methods.** NIST latex calibration standards and Soluplus<sup>®</sup> samples, 0.1, 0.5, 1.0, 2.0, 5.0, and 10.0 % (w/w), were evaluated for their hydrodynamic effective diameter. The calibration standards were evaluated at 25.0 °C and the Soluplus<sup>®</sup> samples were evaluated for their temperature dependence from 15.0 °C to 32.0 °C. Each sample was analyzed with the standard operating procedures shown in Table 6, where the average effective diameter of three 120-s measurements is obtained. The process was run in triplicate for the purpose of determining and reporting uncertainties, where the average of three 120-s measurements was considered a single run.

Before measurement, each sample was filtered using a Sartorius Ministart NML Plus Syringe Filter, with a 0.7 $\mu$ m glass filter, to remove any large aggregates in solution. The filter

was primed twice with sample solution, using the filterings to rinse the cuvette, and the sample was filtered three times. A dust rejection algorithm was also used to remove data resulting from dust and large aggregates in sample. The appropriate dust rejection range is selected based off expected particle size and for multimodal distribution is based off the largest population of particles in sample.<sup>43</sup> The samples were first evaluated using the viscosity and refractive index of water, then recomputed to the experimentally determined viscosity and refractive index of Soluplus<sup>®</sup> samples.

Table 6. Standard operating procedures for temperature dependent particle size analysis.

Parameter	Value
Starting Temperature	15.0 °C
Final Temperature	32.0 °C
Temperature Increment	1.0 °C
Set Duration	120 s
Equilibration Time	300 s
Total Measurements	3
Time Between Measurements	0.0 s
Dust Rejection	50 nm to 250 nm
Fluid	Water
Viscosity	0.890 cP
Refractive Index	1.331
Measurement Angle	90°

## CHAPTER 3. RESULTS AND DISCUSSION

### 3.1 Temperature Dependent Viscoelastic Behavior of Soluplus® Solutions

Calibration standards were analyzed by the rheometer to ensure the instrument's accuracy. The specification on viscosity accuracy is  $\pm 1.0\%$  of full scale range at a specified spindle and speed. The Brookfield viscosity standard fluids are also accurate to  $\pm 1.0\%$  of their stated value. Total allowed error was calculated by summing the deviations from the instrument and fluid, as portrayed by Brookfield (Table 7).<sup>31</sup> Figure 23 shows each standard as a function of temperature and the experimental viscosity values at 25.0 °C.

Table 7. Total allowed error for each viscosity standard fluid at 25.0 °C.

Standard (cP)	Allowed Error (cP)	Experimental Viscosity (cP)
352.4	$\pm 19.87$	350.27
3439	$\pm 132.69$	3,328.83

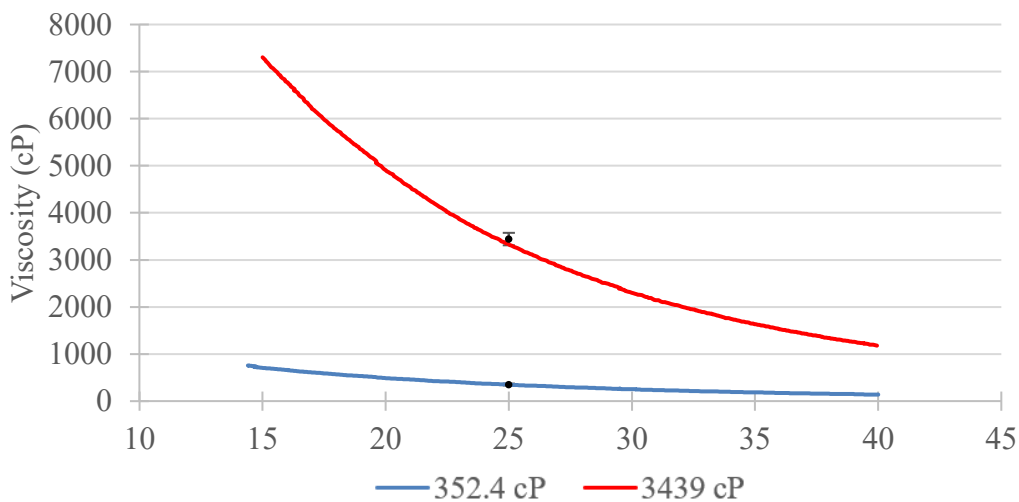


Figure 23. Brookfield viscosity standard fluids as a function of temperature. The solid black points represent the standard's stated viscosity shown with total allowed error.

As shown in Figure 23, at 25.0 °C the 352.4 cP and 3,439 cP standards read 350.27 cP and 3,328.83 cP respectively. Both values were within their allowed deviance from the stated value in Table 7, showing accuracy from the rheometer.

Each concentration of Soluplus<sup>®</sup> samples, ranging 1.0% to 30.0% (w/w), were analyzed three times (Sets 1,2, and 3) by the rheometer for their temperature dependence of viscosity (see Section 2.3.2). Plots of *Viscosity vs Temperature* are shown in Figure 24. For each concentration, a standard deviation was calculated at every 2.0 °C and plotted on the “most representative” run (middle of the three traces). Averaging the sets was not plausible due to varying temperature rates for each run.

The most representative run for each concentration is shown in Figure 25, where each sample is on the same x-axis to better see trends and relationships. There is a general trend in which viscosity decreases to a minimum before rapidly increasing to a maximum. As signified by the solid black tie-line in Figure 25, traces for concentrations above 10.0% exhibit a slight rise in viscosity at low temperatures prior to the decrease toward the minimum. This rise is concentration dependent and can be seen shifting to higher temperatures as concentration increases ( $T_{M1}$ ). Designated by the dashed black line in Figure 25, the steep growth in viscosity to the maximum is essentially concentration independent and occurs around 36.0 °C ( $T_{M2}$ ). The minimum prior to this sharp rise is also essentially concentration independent and occurs around 27.0 °C ( $T_{min}$ ). The temperatures corresponding to these features are listed in Table 8.

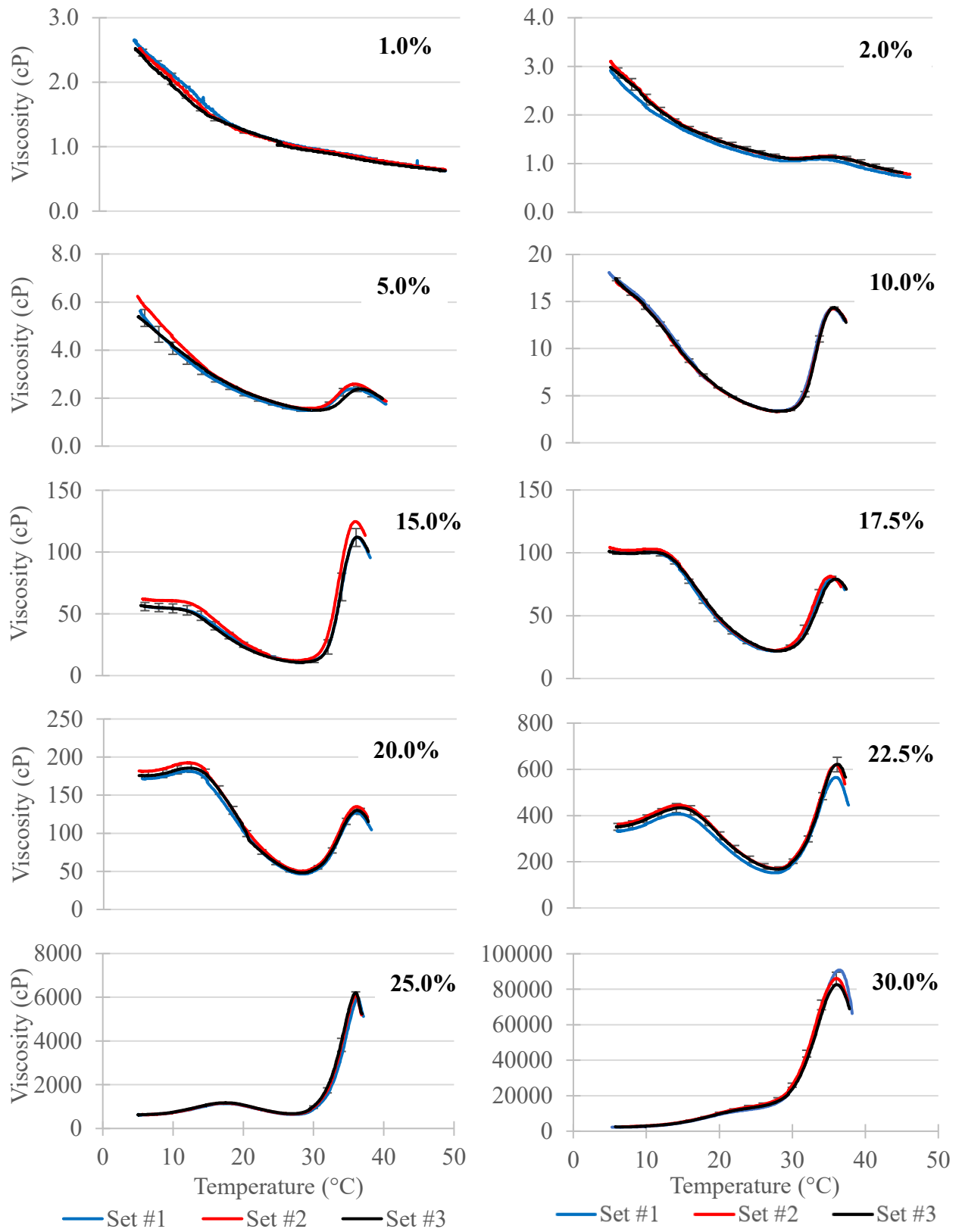


Figure 24. Effect of temperature on viscosity for each aqueous Soluplus<sup>®</sup> sample.

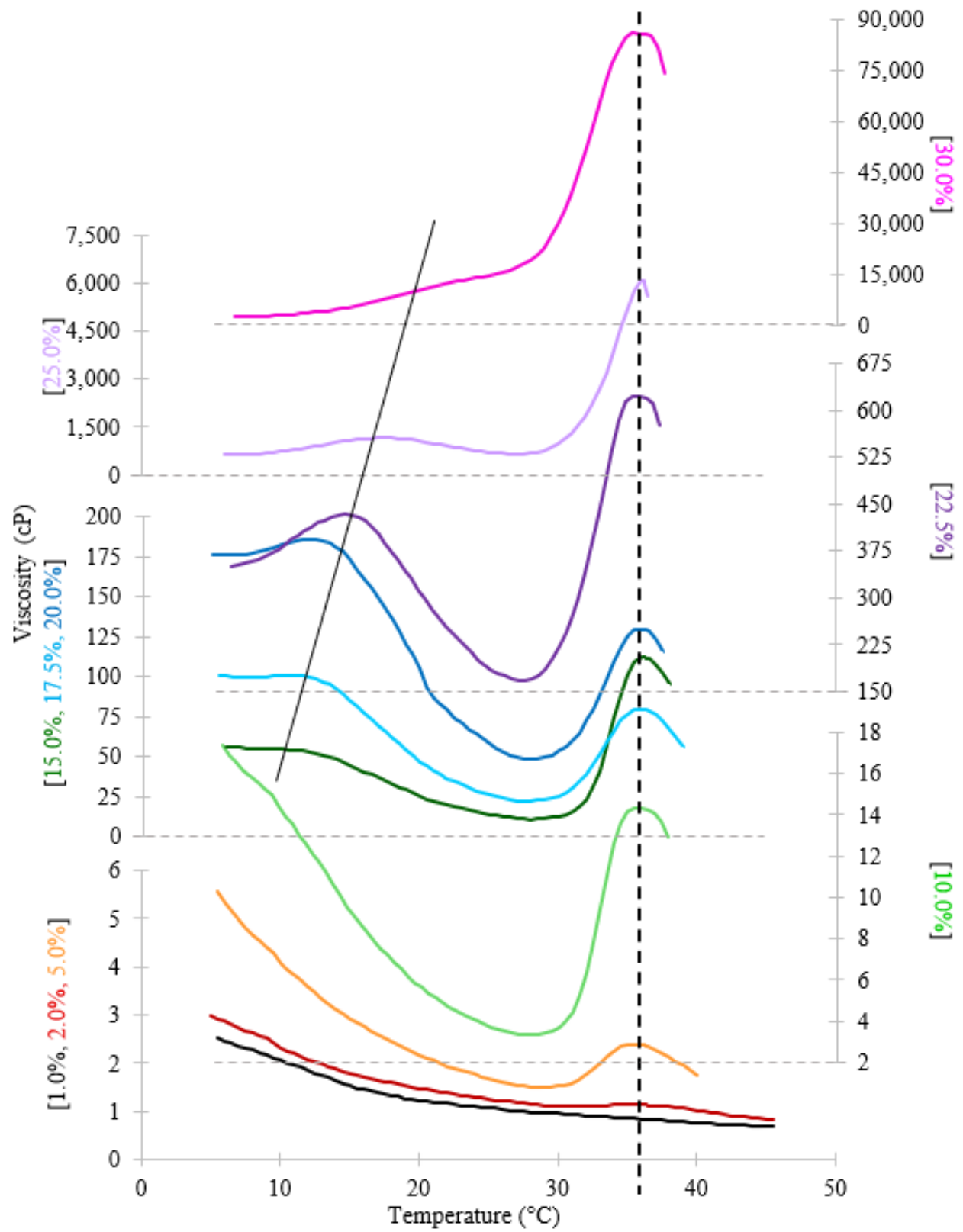


Figure 25. Viscosity of Soluplus® samples on the same temperature scale.

Table 8. Extrema temperatures observed in  $\eta$ - $T$  plots of Soluplus<sup>®</sup> solutions.<sup>†</sup>

Concentration (%)	$T_{M1}$ (°C)	$T_{min}$ (°C)	$T_{M2}$ (°C)
1.0	-	-	-
2.0	-	$30.49 \pm 0.43$	$34.98 \pm 0.23$
5.0	-	$29.28 \pm 0.41$	$35.70 \pm 0.33$
10.0	-	$28.10 \pm 0.07$	$35.86 \pm 0.09$
15.0	$10.54 \pm 0.36$	$27.84 \pm 0.45$	$36.04 \pm 0.17$
17.5	$10.72 \pm 0.26$	$27.96 \pm 0.28$	$35.95 \pm 0.33$
20.0	$12.43 \pm 0.15$	$28.11 \pm 0.03$	$35.87 \pm 0.06$
22.5	$14.75 \pm 0.26$	$27.58 \pm 0.18$	$35.93 \pm 0.13$
25.0	$17.38 \pm 0.18$	$26.99 \pm 0.09$	$36.11 \pm 0.15$
30.0	$22.71 \pm 0.38$	$28.22 \pm 0.77$	$36.18 \pm 0.21$

<sup>†</sup> Uncertainties were determined by averaging the extrema temperature values from Set 1, 2, and 3 and taking the standard deviation.

The sol-gel transition of a thermoresponsive polymer is characterized by an increase in viscosity between the micelle and macrolattice states. As seen in the temperature-dependent plots of viscosity for Soluplus<sup>®</sup> solutions the increase in viscosity takes place from 27.0 °C to 36.0 °C. This sharp increase in viscosity is also seen in literature (Figures 26 and 27) from plots of complex shear viscosity versus temperature. Figure 26 describes the minimum viscosity as an onset of chemical reaction where micelles begin to self-assemble and form superstructures, indicating the beginning of gel formation.<sup>18</sup> Our aqueous Soluplus<sup>®</sup> solutions of varying concentration show this onset of chemical reaction around 27.0 °C (Figures 24 and 25). As the gelling process occurs, viscosity rapidly increases to a sol-gel point. The sol-gel transition is typically defined as the crossing point between  $G'$  and  $G''$  (Figures 26 and 27).<sup>18,29,44</sup> Due to our use of a cone-and-plate rheometer, which is unable to measure  $G'$  and  $G''$  separately, precise sol-gel transitions for our Soluplus<sup>®</sup> solutions were indeterminable. However, as seen in Figure 27, the sol-gel transition occurs within the large increase in viscosity. We hypothesize that the Soluplus<sup>®</sup> sol-gel transition is occurring at a temperature that falls between the average minimum



and average maximum, 27.0 °C to 36.0 °C. To provide a more precise determination of the sol-gel point would require the use of an oscillating rheometer. At 36.0 °C the viscosity of all concentrations reaches its maximum and begins to greatly decrease. At this point, it is hypothesized that the solution has completely gelled and has “broken” inside the rheometer, whereby the cone spindle is no longer able to move through solution. When the solution is at its gel-point, it adheres to the plate in a “solid manner” (Figure 28) causing the spindle to glide against the plate rather than push through solution with resulting force.

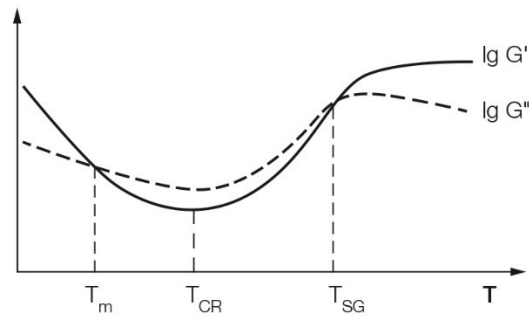


Figure 26. Temperature dependent functions of  $G'$  and  $G''$  for a gelling material (reproduced from Ref. 18).

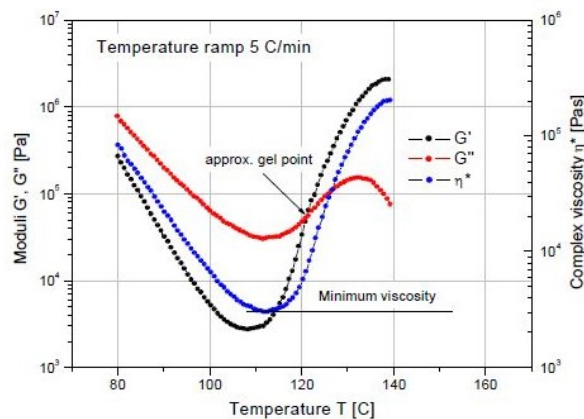


Figure 27. Complex viscosity,  $G'$ , and  $G''$  as a function of temperature for a curing epoxy (reproduced from Ref. 44).



Figure 28. A gelled 20.0% (w/w) Soluplus<sup>®</sup> solution on the plate of a cone-and-plate rheometer. The star-like shape is caused by the pulling away of the CP52 spindle when the solution is gelled. The remaining solution seen circulating around the star-like shape is where the spindle didn't come in contact the plate due to its small diameter.

The concentration-dependent rise in viscosity exhibited at lower temperatures for concentrations above 10.0% (follow the solid black line in Figure 25) is hypothesized to be a physical property of thermoresponsive polymers that has not been described previously. We speculate that it is related to the Krafft point of Soluplus<sup>®</sup> solutions. The Krafft point is the temperature at which the solubility limit of a surfactant is equivalent to the CMC.<sup>45</sup> Therefore, below the Krafft temperature, the surfactant is in a crystalline state and micelles do not form. The visual effect of going below the Krafft temperature is similar to that of clouding, where the surfactant is in a precipitated state and shows opacity.<sup>45</sup> To be described further, as thermoresponsive polymer solutions cloud, they show an increase in viscosity. Therefore, when the polymer solution is below the Krafft point and in a precipitated state, it could be speculated that viscosity would increase as temperature rises to the Krafft point. This is observed in Figure 25 for Soluplus<sup>®</sup> solutions above 10.0%, where the speculated Krafft point would be near the maxima ranging from 11.0 °C to 22.0 °C ( $T_{M1}$  in Table 8). As temperature further increases past these maxima, it is speculated that micelles are forming. The following decrease in viscosity could be due to the switch from having crystals in solution to micelles, or that in general, the

viscosity of Newtonian fluids decreases as temperature increases. At concentrations below 10.0%, it is speculated that the polymer fraction wasn't large enough to witness this slight increase in viscosity or temperatures didn't reach cold enough.

Previous work conducted by our research group reported that aqueous Soluplus<sup>®</sup> solutions physically gel at temperatures from 30.0 °C to 40.0 °C depending on concentration, where more concentrated solutions gel at lower temperatures (Figure 29).<sup>23</sup> This research was conducted using a 90° tilt test and observing at which temperatures the samples stopped flowing. The data obtained by a 90° tilt test roughly matches the rheologically implied temperature range at which the sol-gel transition occurs, 27.0 °C to 36.0 °C. Differences between these sol-gel transition temperature ranges could be from the differences in the experimental processes, where rheology is a more precise way of observing viscoelastic behavior. Figure 29 also reveals that aqueous Soluplus<sup>®</sup> solutions below 10.0% (w/w) do not exhibit a gel phase at any temperature. It is hypothesized that the polymer solutions are not at high enough concentrations for the micelles to interact and form macrolattice structures. Data acquired from the rheometer is at least somewhat consistent with this observation, as seen in the traces from samples under 10.0% (w/w) where the viscosity behavior exhibits small to negligible features that we attribute to the gelation process (Figure 25). We speculate that the small features observed in the 2.0% and 5.0% samples correspond to a pre-gelation condition that does not lead to a complete gelling as measured by the 90 ° tilt test.

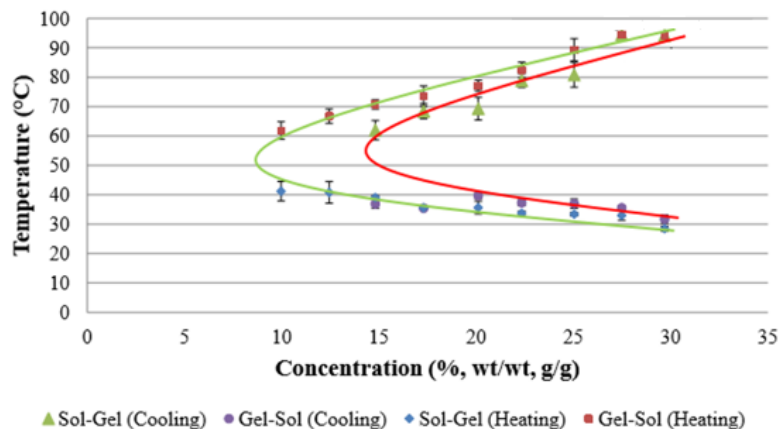


Figure 29. Sol-gel and gel-sol transitions for Soluplus samples as a function of temperature. Speculated phase boundaries (solid lines) have been added to emphasize observed trends (adapted from Ref. 23).

Previous work conducted in our research group also described the cloud-point transitions of Soluplus<sup>®</sup> solutions. The cloud point is described as the transition from soluble to insoluble phases across the LCST phase boundary and has been observed for aqueous Soluplus<sup>®</sup> solutions to be in the range of 27.0 °C to 31.0 °C (Figure 30).<sup>46</sup> The temperature range of cloud transition from previous research lies within the sharp increase of viscosity as did the sol-gel transition. Although these two phase transitions, clouding and gelling, occur at the same temperature range, they are independent of each other. Figures 29 and 30 illustrate the differences in gelling and clouding phase behaviors where the gel point of aqueous Soluplus<sup>®</sup> solutions decreases as a function of increasing concentration, but the cloud point increases as a function of increasing concentration. As previously recognized, Soluplus<sup>®</sup> solutions under 30.0% first experience a cloud transition before physically gelling as a function of increasing temperature. Therefore, it is hypothesized that for aqueous Soluplus<sup>®</sup> solutions below 30.0%, the cloud transition occurs within the temperature range of the sharp viscosity increase (27.0 °C to 36.0 °C), but prior to the gel point.

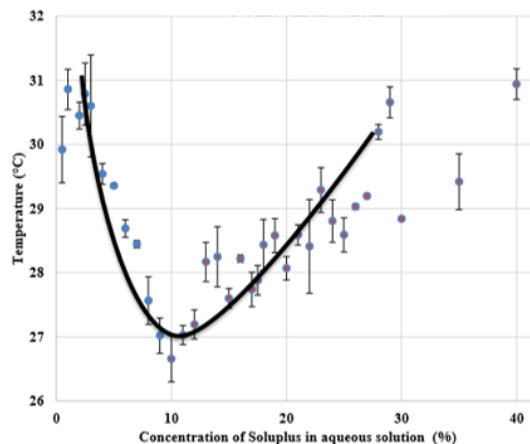


Figure 30. Cloud points for aqueous Soluplus<sup>®</sup> solutions as a function of temperature (reproduced from Ref. 46).

Data from Figure 25 was transformed into a  $\log \text{Viscosity}$  vs.  $\text{Temperature}$  plot to scale all traces onto the same  $x$  and  $y$  axes (Figure 31). The software, Matlab (*Matlab and Simulink* R2019b, MathWorks), was utilized to create a 3-dimensional scatter plot of temperature ( $x$ ), concentration ( $y$ ), and viscosity ( $z$ ). A polynomial model was used to create a least-squares fit of the plotted data where the best fit resulted from a 5<sup>th</sup>-order polynomial in terms of  $x$  and  $y$ , called “Poly55”. As seen in Figure 32, the Poly55 function fits well to low temperatures and low concentrations, however, as viscosity rapidly increases, the function falls far from experimental data. It was decided that because DLS focuses primarily on concentrations below 15.0% and temperatures below 32.0 °C, the least-squares fitting could be confined to only this range of data. As the concentration of Soluplus<sup>®</sup> solutions approaches 0.0% and the viscosity approach that of pure water, the viscosity value will decrease to below the measuring capabilities of our rheometer. Therefore, literature values for the viscosity of water<sup>47</sup> were used to complete the concentration range of 0.0% - 15.0%. Figure 33 shows a Poly54 model (5<sup>th</sup> order in  $x$  and 4<sup>th</sup> order in  $y$ ) that matches closely to the shortened range of data. The Poly55 model was robustly weighted using “Bisquare”, where the weight given to each data point is determined by how far

the point is from the fitted line. This allows for the fit to be based on the bulk data, minimizing any outlier effects.<sup>48</sup> The Poly54 model didn't use robust fitting on top of the polynomial fit.

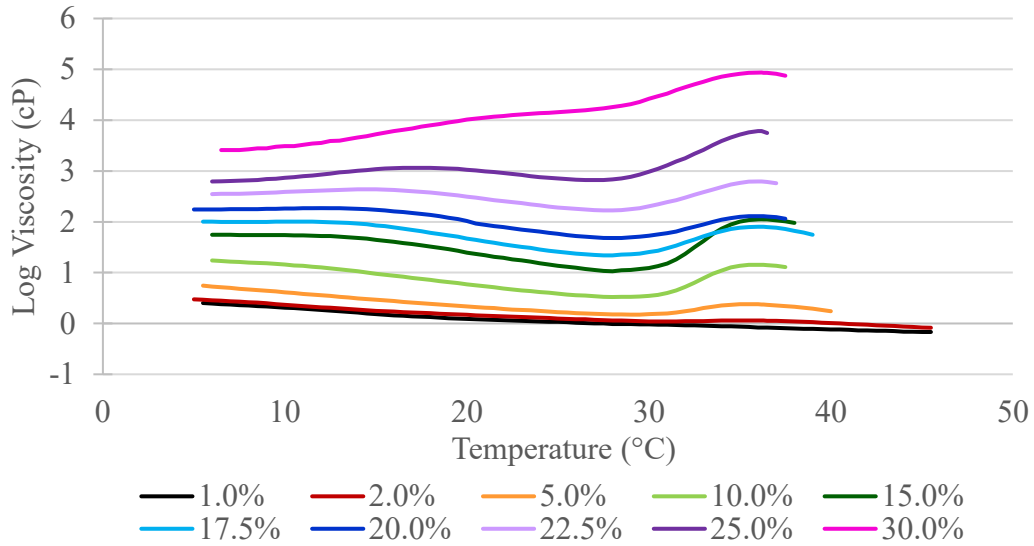


Figure 31. Log-linear plot of viscosity vs. temperature of aqueous Soluplus<sup>®</sup> solutions at different concentrations.

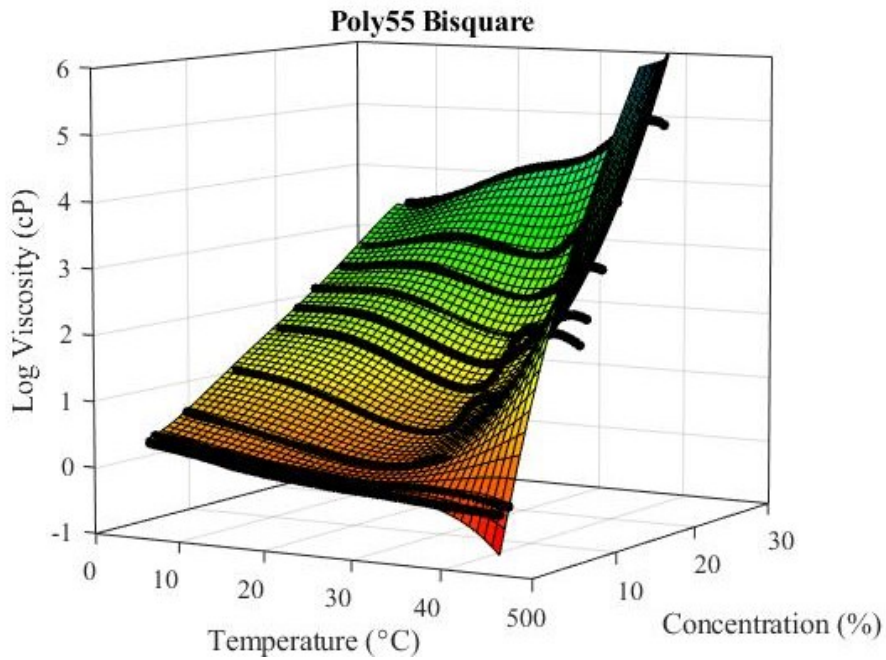


Figure 32. Full range of experimental data modeled with a Poly55-Bisquare fit.

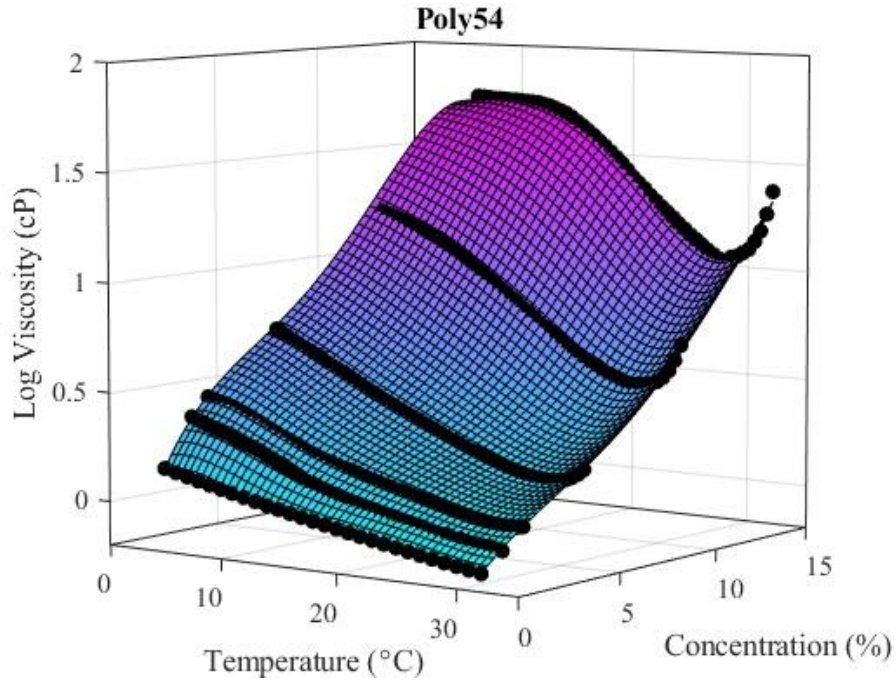


Figure 33. Short range of experimental data modeled with a Poly54 fit.

From the Poly54 modeled fit, a polynomial function was created so that the viscosity of Soluplus<sup>®</sup> samples could be determined for any temperature ranging 5.0 °C to 32.0 °C and concentration ranging 0.0% to 15.0%. The full Poly54 fit function is shown below,

$$\begin{aligned}
 \log(\eta) = & -0.1652 + 0.1448(T) + 0.282(\rho) - 0.02019(T^2) - 0.02223(T)(\rho) & (10) \\
 & - 0.04058(\rho^2) + 0.001153(T^3) + 0.001691(T^2)(\rho) + 0.00144(T)(\rho^2) \\
 & + 0.00414(\rho^3) - 3.02 \times 10^{-5}(T^4) - 7.008 \times 10^{-5}(T^3)(\rho) \\
 & - 3.204 \times 10^{-5}(T^2)(\rho^2) - 7.989 \times 10^{-5}(T)(\rho^3) - 0.0001442(\rho^4) \\
 & + 2.976 \times 10^{-7}(T^5) + 1.043 \times 10^{-6}(T^4)(\rho) + 5.061 \times 10^{-7}(T^3)(\rho^2) \\
 & - 3.19 \times 10^{-7}(T^2)(\rho^3) + 3.344 \times 10^{-6}(T)(\rho^4)
 \end{aligned}$$

where  $\eta$  is viscosity,  $T$  is temperature in Celsius, and  $\rho$  is the relative mass concentration (w/w). Equation 10 shows accuracy to experimental viscosity data within a 3.0% difference around 95% of the time, where the other 5% is within a 10.0% difference (occurring primarily at low concentrations and low temperatures or high concentrations and high temperatures).

### 3.2 Temperature Dependent Refractive Index of Soluplus<sup>®</sup> Solutions

Because particle size analysis by dynamic light scattering depends on viscosity and refractive index, these parameters were evaluated for on Soluplus<sup>®</sup> solutions to ensure accurate hydrodynamic effective diameter measurement. The temperature dependence of viscosity for Soluplus<sup>®</sup> solutions is described in Section 3.1 and the following gives the refractive index behavior of aqueous Soluplus<sup>®</sup> solutions as a function of temperature.

Water and ethanol were evaluated at 20.0 °C by the 2WAJ Abbe refractometer to check the instrument's accuracy. The refractometer has a specified accuracy of  $\pm 0.0002$ , and the experimental results can be seen in Table 9 compared to literature values. The refractive index of ethanol is within the allowed deviation of its literature value, but the value of water lies 0.0006 away from its literature value. Since the effect of refractive index on particle size analysis is relatively weak (see Section 3.3), it was concluded that this deviation can be tolerated. Furthermore, the NanoBrook Omni instrument considers refractive index to only the thousands place, so the observed deviation is within the natural precision of the correction.

Table 9. Experimental and literature refractive index values for water and ethanol at 20.0 °C.

Standard	Refractive Index ( <i>n</i> ) at 20.0 °C	
	Experimental	Literature
Water	1.3324	1.3330 <sup>d</sup>
Ethanol	1.3612	1.3611 <sup>e</sup>

<sup>d</sup> from Ref. 49

<sup>e</sup> from Ref. 50

Each concentration of Soluplus<sup>®</sup> solution, ranging 0.1% to 10.0% (w/w), were evaluated for their refractive index from 11.0 °C to 35.0 °C as described in Section 2.4.2. These data can be



seen in Figure 34, where the 0.1% trace included representative standard deviations as determined from repetitive runs. As shown in the figure, refractive index increases as the concentration of Soluplus<sup>®</sup> increases. As well, the refractive index decreases slowly as temperature increases for all concentrations. This trend replicates the refractive index behavior of pure water.<sup>49</sup>

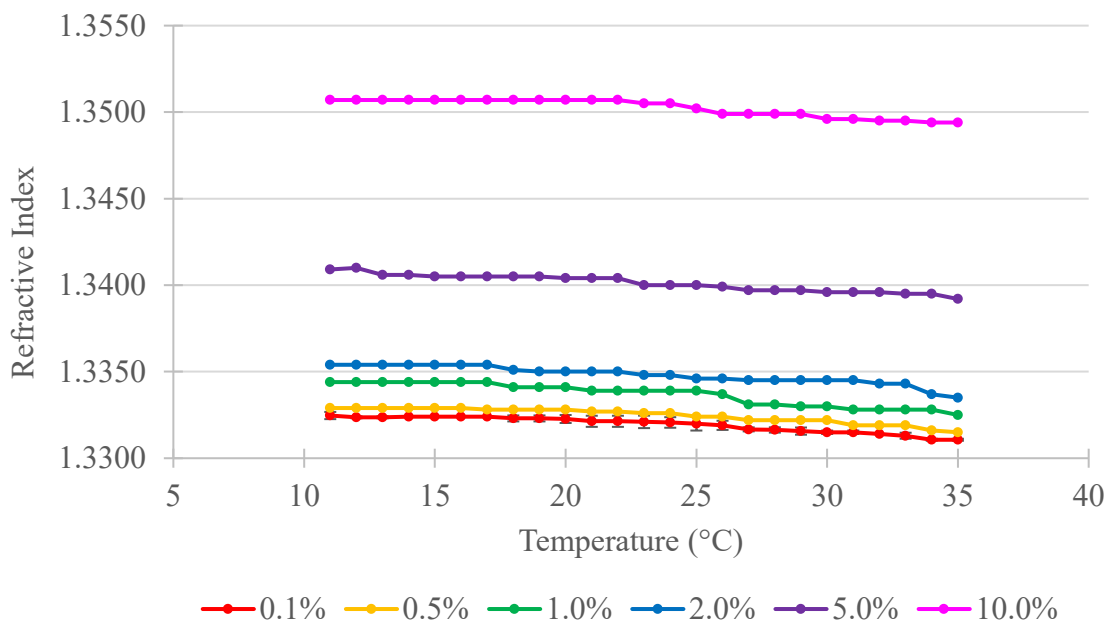


Figure 34. Effect of temperature on refractive index for Soluplus<sup>®</sup> samples.

### 3.3 Particle Size Analysis of Soluplus<sup>®</sup> Solutions

Calibration standards were evaluated by the NanoBrook Omni particle size analyzer to ensure the instrument's accuracy. NIST specifies that their latex calibration standards do not come with a pass/fail criterion due to underlying sizing methodology that is customer dependent.<sup>51</sup> NIST recommends establishing an in-house criterion to test instrument performance, which has been adopted as  $\pm 4.00$  nm in the chemistry department at Missouri

State University.<sup>52</sup> The experimental hydrodynamic effective diameters of the 42.9 nm and 288 nm standards can be seen in Table 10, where it is shown that our measurements pass in-house criteria, displaying good instrument performance. The polydispersity index (PDI) is also included in Table 10, which signifies the relative size-range of particles. The PDI can range from 0.000 to 1.000, where a lower value corresponds to a more monodisperse sample.

Table 10. Effective diameters of NIST latex calibration standards at 25.0 °C.

Standard (nm)	Experimental Eff. Diam. (nm)	Experimental Polydispersity
42.9	45.92	0.106
288	285.8	0.040

Soluplus<sup>®</sup> solutions, 0.1%, 0.5%, 1.0%, 2.0%, 5.0%, and 10.0% (w/w), were each evaluated three times (Sets 1, 2, and 3) for their hydrodynamic effective diameters as a function of temperature using the NanoBrook Omni particle size analyzer following the protocol in Section 2.5.2. Figure 35 displays the average hydrodynamic effective diameters, along with uncertainties, for each sample as a function of temperature using “uncorrected” viscosity and refractive index data. “Uncorrected” refers to using the pre-programmed viscosity and refractive index data for a pure water solvent. As observed, the temperature dependence generally shows the diameter to decrease with increasing temperature and then sharply rise as the cloud- or gel-point is reached. Additionally, the effective diameter appears to be directly proportional to Soluplus<sup>®</sup> concentration, in that for any given temperature the largest particle diameter is obtained for the highest Soluplus<sup>®</sup> concentration. The sharp rise in the temperature dependence of the hydrodynamic effective diameter appears to correlate with the solution’s clouding or gelling point, where micelles are aggregating and produce larger particles. The 0.1% and 0.5%

Soluplus<sup>®</sup> samples don't show this sharp rise in diameter, suggesting that there is no onset of physical change. However, according to Figure 30, these concentrations do show clouding by spectroscopy, whereas they do not show evidence gelling (Figure 29).

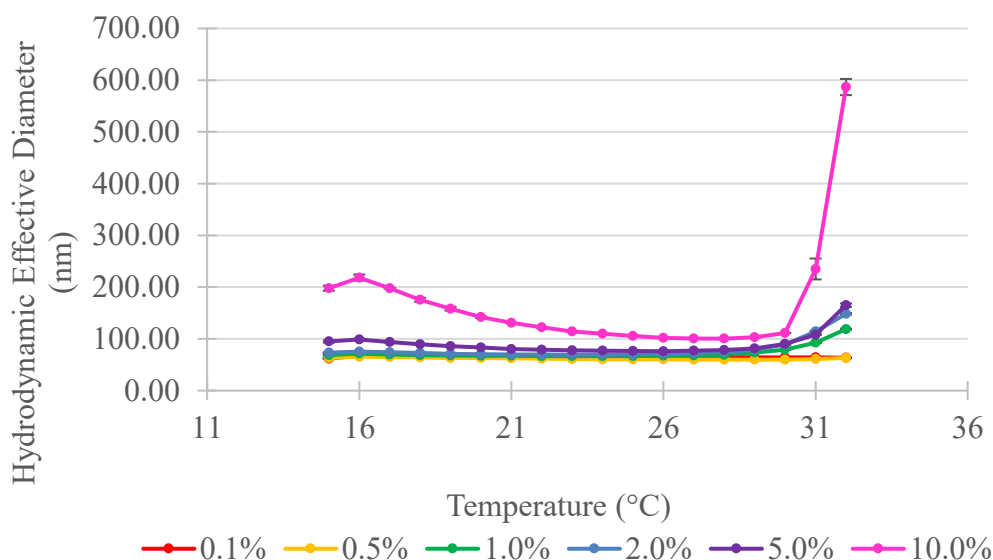


Figure 35. Effect of temperature on effective diameter for Soluplus<sup>®</sup> solutions using uncorrected values of viscosity and refractive index.

The traces in Figure 35 were recomputed to correct for the viscosity and refractive index behavior of Soluplus<sup>®</sup> solutions. In the following discussion, “corrected” refers to using the viscosity and refractive index data of Soluplus<sup>®</sup> solutions reported in Sections 3.1 and 3.2. As seen in Figure 36, the corrected effective diameters are observed to be inversely proportional to concentration. Figure 37 depicts this trend for one specific temperature (25.0 °C) by comparing hydrodynamic diameters obtained from “uncorrected” vs. “corrected” analyses. Table 11 gives the numerical values shown in Figure 37 along with PDI values. It is notable that the PDI shows no dependence on viscosity or refractive index. It is reported in literature that the cause for the decreasing diameter as concentration increases is related to micellar core size. At larger

concentrations, micelles form with less solvent in the core, causing the micelle to compact and reduce in size.<sup>6</sup>

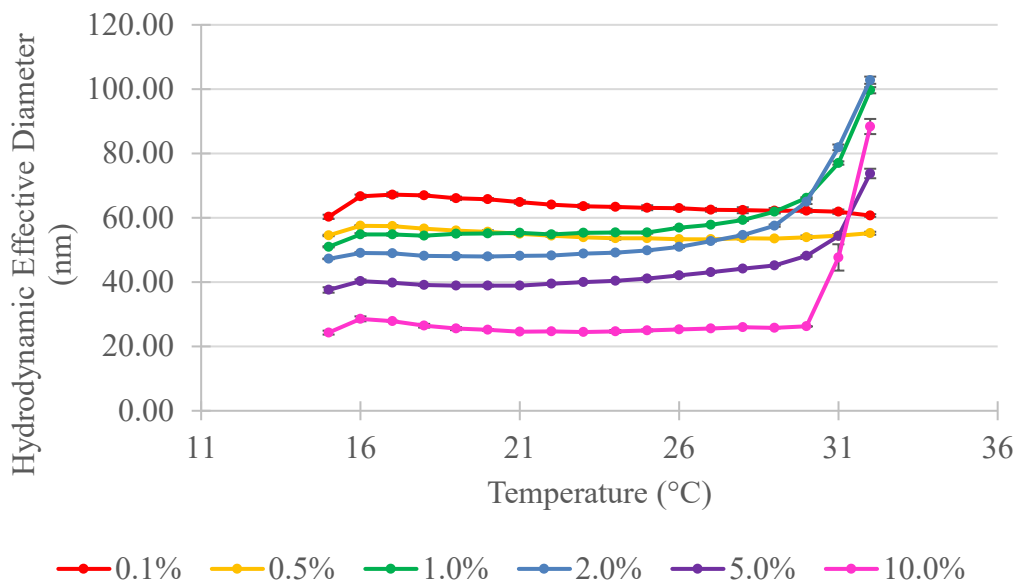


Figure 36. Effect of temperature on effective diameter for Soluplus<sup>®</sup> solutions using corrected values of viscosity and refractive index.

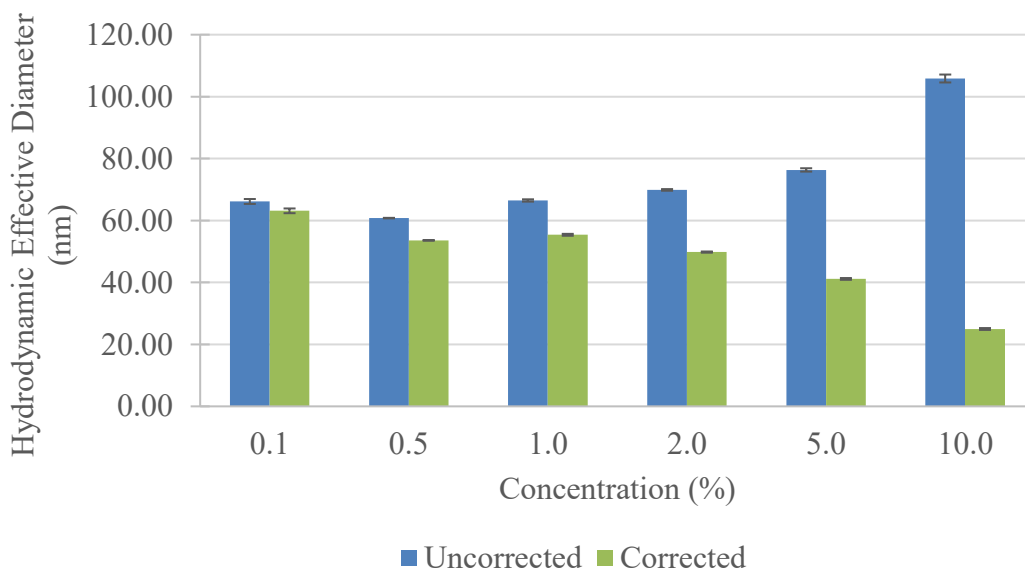


Figure 37. Uncorrected vs. corrected diameter at 25.0 °C for Soluplus<sup>®</sup> in aqueous solution.

Table 11. Uncorrected vs. corrected effective diameters at 25.0 °C for Soluplus® in aqueous solution.

Concentration (%)	Hydrodynamic Effective Diameter (nm)		
	Uncorrected	Corrected	Polydispersity
0.1	66.15 ± 0.79	63.13 ± 0.76	0.030
0.5	60.78 ± 0.08	53.59 ± 0.06	0.038
1.0	66.48 ± 0.37	55.39 ± 0.31	0.042
2.0	69.88 ± 0.26	49.81 ± 0.19	0.059
5.0	76.34 ± 0.54	41.14 ± 0.29	0.103
10.0	105.85 ± 1.28	24.98 ± 0.30	0.210

Also depicted in Figure 36, the “corrected” diameter values remain more consistent through rises in temperature prior to sharply increasing. As well, the sharp rise in effective diameter remains around the same temperature. The 0.1% and 0.5% Soluplus® samples were recomputed using extrapolated viscosities as determined by Equation 10. The Brookfield RVDV-III Ultra rheometer was unable to test these low concentrated samples because their viscosities fall below the instrumental limit. It is suspected that because these viscosity values were extrapolated from outside the experimentally determined range, the resulting corrected diameters may contain an inherently higher level of uncertainty. In Figure 36, the 0.1% and 0.5% traces still show no evidence for physical phase change by DLS (*i.e.*, a sharp increase in diameter at higher temperatures).

Salah, et. al., report the hydrodynamic diameter of Soluplus® in a 0.1% (w/w) aqueous solution at 20.0 °C to be 64.86 ± 1.58 nm (Figure 38).<sup>15</sup> The experimentally determined “corrected” effective diameter from this thesis for an equivalent sample under the same conditions is 65.76 ± 0.38 nm (Figure 36), consistent with the previously reported value.

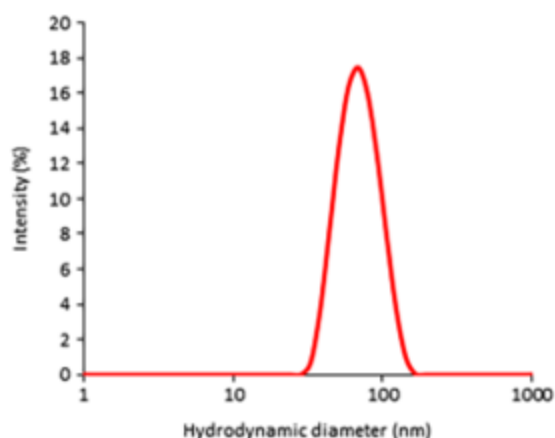


Figure 38. Size distribution for a 0.1% Soluplus<sup>®</sup> solution at 20.0 °C (reproduced from Ref. 15).

The influence of including accurate viscosity and refractive index data in particle size algorithms is considerable. For example, the hydrodynamic effective diameter shifts from 143.48 nm to 25.35 nm for the 10.0% Soluplus<sup>®</sup> solution at 20.0 °C upon correcting for these effects (Table 12). This substantial shift (82.3% decrease) on diameter is due primarily to viscosity effects. Refractive index plays a less significant role in particle size analysis by DLS. As shown in Table 13, the resulting hydrodynamic diameter in a 10.0% Soluplus<sup>®</sup> solution is shifted only 1.50% by changing refractive index by 0.010, indicating that the correction due to refractive index variation is significantly less important than that due to viscosity.

Table 12. Difference in effective diameter when using uncorrected and corrected viscosity and refractive index data for a 10.0% Soluplus<sup>®</sup> solution at 20.0 °C.

SOP	Uncorrected	Corrected
Liquid	Water	Unspecified
Viscosity (cP)	1.002	5.842
Refractive Index	1.331	1.351
Effective Diameter (nm)	143.48	25.35

Table 13. Effective diameter dependence on refractive index for a 10.0% Soluplus<sup>®</sup> solution at 20.0 °C and 5.842 cP.

Refractive Index	Effective Diameter (nm)
1.341	24.98
1.351	25.35
1.361	25.73

As discussed previously, the sharp increase in effective diameter that is observed for the 1.0%, 2.0%, 5.0%, and 10.0% (w/w) Soluplus<sup>®</sup> solutions is related to the cloud- or gel-point. Figure 39 overlays the viscosity and effective diameter of a 5.0% Soluplus<sup>®</sup> solution on the same temperature axis. As observed, effective diameter remains relatively constant as viscosity is decreasing to its minimum across the temperature range. As viscosity starts to increase, indicating an onset of change (clouding, gelling, or both), the effective diameter also rises. The increase in particle size is triggered by the reduced solubility of solution as it crosses the LCST phase boundary. This causes the micelles to aggregate and rearrange, resulting in larger and more polydisperse particle sizes.<sup>15</sup>

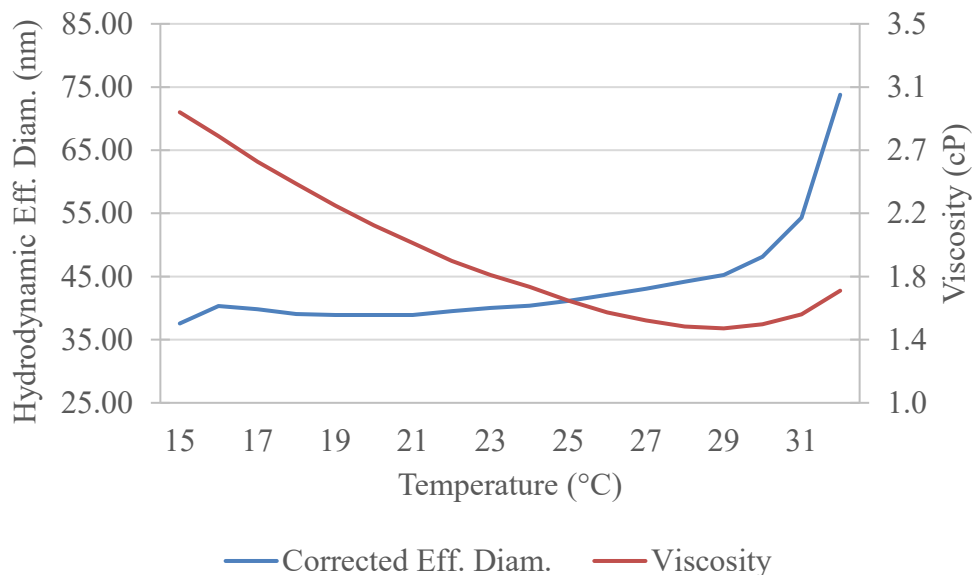


Figure 39. Viscosity and corrected diameter vs. temperature for a 5.0% Soluplus<sup>®</sup> solution.

## CHAPTER 4. CONCLUSIONS AND FUTURE DIRECTIONS

The phase behavior of aqueous solutions of Soluplus<sup>®</sup>, a polyvinyl caprolactam-polyvinyl acetate-polyethylene glycol graft copolymer, were studied throughout this research.

Rheologically determining the effect of temperature on viscosity allowed for insight behind the viscoelastic properties of thermothickening polymer solutions. It was observed that as temperature rises, the viscosities of Soluplus<sup>®</sup> solutions decrease until reaching a minimum around 28.0 °C where viscosity then sharply increases. This trend has been observed by other researchers for gelling polymers where a large increase in viscosity signifies the agglomeration of polymeric micelles into macrolattices. The sharp increase in viscosity for aqueous Soluplus<sup>®</sup> solutions is concentration independent and occurs from 27.0 °C to 36.0 °C. Within this temperature range, polymeric micelles aggregate into a network and gel, but determining a specific gel-point is unattainable with use of a cone-and-plate rheometer. A precise gel-point could be determined by use of an oscillatory rheometer. The temperature at which viscosity sharply rises is also seen to correlate with cloud point, where the solution is in an insoluble phase and micelles begin to rearrange and agglomerate due to decreased solubility. Although gelling and clouding both occur around the same temperature, they show no evidence of true correlation. The cause of swelling in viscosity seen at lower temperatures for concentrations above 10.0% remains inconclusive, however, we speculate that this is due to the Krafft point of aqueous Soluplus<sup>®</sup> solutions. We hypothesize that the Krafft point temperature, where micelles begin to form, is where viscosity begins to increase. With further analysis on particle size this behavior could be better interpolated. For example, studying the particle size of a 20.0% (w/w) Soluplus<sup>®</sup> solution from 5.0 °C to 20.0 °C would show micelle behavior before and after the viscosity



increase. If the particle size in solution increases as viscosity increases, a physical phase behavior would be witnessed. Possibly, going from a crystalline to micelle state due to the Krafft point.

Particle size algorithms used in DLS analyses are directly dependent on viscosity and refractive index values of the solutions. Therefore, it is important to include accurate information for these parameters. In this thesis, a relationship between concentration, temperature, and viscosity was determined by measuring sets of these variable and fitting the data to a 2-variable polynomial function. From this equation, accurate viscosity values could be identified and used in particle size analysis for Soluplus<sup>®</sup> solutions. The refractive index of Soluplus<sup>®</sup> solutions were studied and showed close similarity to that of water, where refractive index decreases slightly as a function of increasing temperature. The effect of refractive index on hydrodynamic effective diameter is minimal in DLS. However, viscosity plays a much more significant role, where a 4.840 cP increase in viscosity caused effective diameter to decrease 82.3%.

The hydrodynamic effective diameter of Soluplus<sup>®</sup> particles in aqueous solution, as measured by DLS, changed significantly upon application of corrections due to viscosity and refractive index effect. The most significant difference observed after the corrections was in the relationship between concentration and effective diameter, where the uncorrected trend of particle size increasing with concentration proved to be the opposite trend (particle size *decreases* with increasing concentration) after corrections were applied.

For a given concentration, plots of hydrodynamic effective diameter *vs.* temperature showed an overall decrease with temperature to a minimum near 27.0 °C, followed by a sharp rise around 30.0 °C for all concentrations. This rise in diameter appears to correlate with the solutions phase behaviors, clouding and gelling.

Soluplus<sup>®</sup> is a tri-block graft copolymer that is used in the pharmaceutical industry to enhance the bioavailability of APIs, by encapsulating insoluble drugs within a micellar core. Studying the effect of temperature on particle size and viscoelastic behavior gives insight to how the polymeric micelles will behave once subjected to body temperature. Supported by this research, Soluplus<sup>®</sup> shows interest in the biomedical field as a drug carrier system, through its thermoresponsive behaviors in viscoelasticity and particle size.

## REFERENCES

- 1 S. Koltzenburg, in *Solubility Enhancement with BASF Pharma Polymers*, ed. T. Reintjes, BASF SE, Lampertheim, Germany, 2011, 1, 9-26.
- 2 M. A. Ward and T. K. Georgiou, *Polymers*, 2011, **3**, 1215-1242.
- 3 D. W. van Krevelen and K. te Nijenhuis, *Properties of Polymers*, Elsevier, Amsterdam, Netherlands, 2009.
- 4 S. Okabe, S. Sugihara, S. Aoshima and M. Shibayama, *Macromolecules*, 2003, **36**, 4099-4106.
- 5 Y. Tanaka, in *Rheology*, ed. J. D. Vicente, InTech, Rijeka, Croatia, 2012, 2, 29-58.
- 6 S. S. Kulthe, Y. M. Choudhari, N. N. Inamdar and V. Mourya, *Designed Monomers and Polymers*, 2012, **15**, 465-521.
- 7 J. F. Alopaeus, E. Hagesaether and I. Tho, *Pharmaceuticals*, 2019, **12**, 1-23.
- 8 R. Tanbour, A. M. Martins, W. G. Pitt and G. A. Hussein, *Current Pharmaceutical Design*, 2016, **22**, 1-12.
- 9 G. P. Andrews and D. S. Jones, *Biomacromolecules*, 2006, **7**, 899-906.
- 10 K. Yotsumoto, K. Ishii, M. Kokubo and S. Yasuoka, *Int. J. Pharm.*, 2018, **553**, 132-140.
- 11 A. Gandhi, A. Paul, S. O. Sen and K. K. Sen, *Asian J. Pharm. Sci.*, 2015, **10**, 99-107.
- 12 The Science of Insolubility-BASF, <https://themedicinemaker.com/discovery-development/the-science-of-insolubility>, (accessed November 2019).
- 13 Y. Zhu, R. Batchelor, A. B. Lowe and P. J. Roth, *Macromolecules*, 2016, **49**, 672-680.
- 14 R. Hoogenboom, in *Smart Polymers and Their Applications*, ed. M. R. Aguilar and J. S. Roman, Woodhead Publishing, Sawston, Cambridge, 2014, 2, 19.
- 15 I. Salah, M. Abou Shamat and M. T. Cook, *J. Appl. Polym. Sci.*, 2019, **136**, 46915.
- 16 The IUPAC Compendium of Chemical Terminology, <https://goldbook.iupac.org/>, (accessed October 2019).
- 17 Soluplus Technical Information-BASF, <https://pharmaceutical.basf.com/en/Drug-Formulation/Soluplus.html>, (accessed September 2019).

- 18 D. Djuric, in *Solubility Enhancement with BASF Pharma Polymers*, ed. T. Reintjes, BASF SE, Lampertheim, Germany, 2011, 5, 67-68.
- 19 Soluplus<sup>®</sup>-The Solid Solution, <https://pharmaceutical.basf.com/en/Drug-Formulation/Soluplus.html>, (accessed November 2019).
- 20 L. Di and E. H. Kerns, in *Drug-Like Properties: Concepts, Structure, Design, and Methods*, Academic Press, Cambridge, Massachusetts, 2<sup>nd</sup> edition, 2016, 19, 267-281.
- 21 Soluplus<sup>®</sup> Regulatory Facts Sheet, <https://www.pharmaexcipients.com/news/soluplus-is-approved-in-generics-in-taiwan-and-argentina-and-is-now-filed-in-brazil/>, (accessed November 2019).
- 22 G. Bonacucina, M. Cespi, G. Mencarelli, G. Giorgioni and G. F. Palmieri, *Polymers*, 2011, **3**, 779-811.
- 23 K. Kosinska, Non-Thesis Degree Paper, Department of Chemistry, Missouri State University, 2016.
- 24 C. M. Reynolds, unpublished work, 2013.
- 25 J. Stetefeld, S. A. McKenna and T. R. Patel, *Biophys. Rev.*, 2016, **8**, 409-427.
- 26 DLS Technical Note [MRK656-01]-Malvern Instruments, [https://warwick.ac.uk/fac/cross\\_fac/sciencecity/programmes/internal/themes/am2/booking/particlesize/intro\\_to\\_dls.pdf](https://warwick.ac.uk/fac/cross_fac/sciencecity/programmes/internal/themes/am2/booking/particlesize/intro_to_dls.pdf), (accessed November 2019).
- 27 Technical Note Viscosity Effects-Horiba, <http://www.horiba.com/fileadmin/uploads/Scientific/Documents/PSA/TN140.pdf>, (accessed September 2019).
- 28 Brookfield Engineering Laboratories Inc., *More Solutions to Sticky Problems*, Brookfield, Middleboro, MA, 2014.
- 29 T. G. Mezger, *The Rheology Handbook: For users of rotational and oscillatory rheometers*, Vincentz Network, Hanover, Germany, 2014.
- 30 D. L. Blair, in *Molecular Gels: Structure and Dynamics*, ed. R. G. Weiss, Royal Society of Chemistry, London, United Kingdom, 2018, 2, 28-32.
- 31 Brookfield Engineering Laboratories Inc., *Brookfield DV-III Ultra Programmable Rheometer Operating Instructions: Manual No. M/98-211-B0104*, Brookfield, Middleboro, MA.
- 32 N. Merlet-Lacroix, E. D. Cola and M. Cloitre, *Soft Matter*, 2010, **6**, 984-993.

- 33 Viscosity of Adhesives, <https://www.galindberg.se/blogg/viscosity-of-adhesives/>, (accessed November 2019).
- 34 Basics of Rheology-Anton Paar, <https://wiki.anton-paar.com/us-en/basics-of-rheology/#rheology-and-rheometryrelated-information>, (accessed November 2019).
- 35 The provided Soluplus® expired in May 2017, but there is no evidence of complication due to expiration.
- 36 Rheometers vs Viscometers-Malvern Panalytical, <https://www.malvernpanalytical.com/en/products/measurement-type/viscosity/rheometer-vs-viscometer>, (accessed October 2019).
- 37 Rheometers-Malvern Panalytical, <https://www.malvernpanalytical.com/en/products/category/rheometers>, (accessed October 2019).
- 38 P. Fernanda, in *Structure-Function Analysis of Edible Fats*, ed. A. G. Marangoni, Elsevier, Amsterdam, Netherlands, 2<sup>nd</sup> Edition, 2018, 11, 313-385.
- 39 Rheometers-How do they compare?, <https://www.atascientific.com.au/rheometers-compare/>, (accessed October 2019).
- 40 J. W. Goodwin and R. W. Hughes, *Rheology for Chemists: An Introduction*, Royal Society of Chemistry, London, United Kingdom, 2008.
- 41 Abbe Refractometer-ChemBuddy, <http://www.refractometer.pl/Abbe-refractometer>, (accessed January 2020).
- 42 The NIST traceable particle size standards expired as of June 2019, but show no evidence of complication due to expiration.
- 43 NanoBrook Omni Brochure-Brookhaven Instruments, <https://www.brookhaveninstruments.com/wp-content/uploads/2019/10/NanoBrook-Omni.pdf>, (accessed January 2020).
- 44 Thermosetting Polymers-Rheological Testing, <https://www.azom.com/article.aspx?ArticleID=12103>, (accessed December 2019).
- 45 Y. Nakama, in *Cosmetic Science and Technology: Theoretical Principles and Applications*, Elsevier, Amsterdam, Netherlands, 2017, 15, 231-244.
- 46 R. Balzam, Master's Thesis, Missouri State University, 2016.
- 47 Viscosity of Water, <https://wiki.anton-paar.com/us-en/water/>, (accessed January 2020).
- 48 Least-Squares Fitting: MathWorks®, <https://www.mathworks.com/help/curvefit/least-squares-fitting.html>, (accessed January 2020).

- 49 A. N. Bashkatov and E. A. Genina, *Proc. of SPIE*, 2003, **5068**, 393-395.
- 50 U.S. National Library of Medicine-PubChem, <https://pubchem.ncbi.nlm.nih.gov/compound/Ethanol>, (accessed January 2020).
- 51 Precision Particles: NIST Traceable Size Standards [TDS 623]-Polysciences Inc., <https://www.polysciences.com/skin/frontend/default/polysciences/pdf/TDS%20623.pdf>, (accessed February 2020).
- 52 In-house standard deviation criteria was created by testing fresh sets of the NIST traceable particle standards on various days, with various methods of sample preparation. For the 42.9 nm standard, six samples were tested and had an average effective diameter of  $45.43 \pm 1.46$  nm. The 288 nm standard gave an average effective diameter of  $288.2 \pm 2.17$  nm with three samples tested. It was decided that any standard within  $\pm 4.00$  nm from the stated true particle size was acceptable.